Available online at www.sciencedirect.com

ScienceDirect

Geochimica et Cosmochimica Acta 248 (2019) 61–87

Geochimica et Cosmochimica Acta

www.elsevier.com/locate/gca

Coupled mineral alteration and oil degradation in thermal oil-water-feldspar systems and implications for organic-inorganic interactions in hydrocarbon reservoirs

Guanghui Yuan [a,b,*], Yingchang Cao [a,*], Nianmin Zan [a], Hans-Martin Schulz [c], Jon Gluyas [d], Fang Hao [a], Qiang Jin [a], Keyu Liu [a], Yanzhong Wang [a], Zhonghong Chen [a], Zhenzhen Jia [a]

[a] *Key Laboratory of Deep Oil and Gas, School of Geosciences, China University of Petroleum, Qingdao 266580, China*

[b] *Laboratory for Marine Mineral Resources, Qingdao National Laboratory for Marine Science and Technology, No. 62, Fuzhou South Road, Qingdao 266071, China*

[c] *GFZ German Research Centre for Geosciences, Section 4.3, Organic Geochemistry, Telegrafenberg, D-14473 Potsdam, Germany*

[d] *Department of Earth Sciences, Durham University, Durham DHs 3LE, UK*

Received 19 January 2018; accepted in revised form 2 January 2019; available online 11 January 2019

Abstract

Organic-inorganic interactions after oil charging are critical for determining the ongoing evolution of hydrocarbons and rock quality in water-wet siliciclastic reservoirs. It is the conceptual approach of this study to simulate and decipher these interactions by using quantitative analyses of the interrelated changes of minerals, water, hydrocarbons, gases, and organic acids in heated oil-water-rock systems.

The experimental results show that organic-inorganic interactions occur between the organic oil and inorganic feldspar in the presence of water. Water promotes the oil degradation by an extra supply of H^+ and OH^- ions. In the oil-water-rock systems, mutual exchanges of H^+ and OH^- ions among minerals, water, and hydrocarbons probably result in the mutual interactions between oil degradation and mineral alteration, with water serving as a matrix for the ion exchange. In the oil-water-feldspar system, feldspar alteration does not cease in the oil zone in the presence of some water and, inversely, oil degradation can even accelerate the alterations of the aluminosilicate minerals. The mineral alterations from feldspar to boehmite, illite, and muscovite promote the oil degradation in the oil-deionized water-feldspar systems with the mutual ion exchange. Due to a possible competition between the Brønsted acid sites in the minerals and the halide anions or the direct replacement of K-feldspar by albite, the mineral alterations retard the oil degradation in the oil-NaCl water-feldspar systems. The experimental results also indicate that oil degradation via free radical cross-linking and free radical thermal cracking is extensive in anhydrous oil systems and may lead to blocking of pores and throats by the generated pyrobitumen in the oil zone of a reservoir. In contrast, in the oil-water transition zone of a reservoir, oil degradation via thermal cracking and oxidative decomposition may dominate the oil degradation and may lead to the generation of secondary pores with leaching of minerals by the generated CO_2 and organic acids.

This study demonstrates that organic-inorganic interactions are complex and proceed in diverse pathways in different hydrogeochemical systems. Thus, further quantitative investigations of the reaction pathways and reaction kinetics of coupled mineral alteration and oil degradation in oil-water-rock systems are warrented. Meanwhile, the incorporation of such organic-

* Corresponding authors at: School of Geosciences, China University of Petroleum, Qingdao 266580, China (G. Yuan).
E-mail addresses: yuan.guanghui@upc.edu.cn (G. Yuan), caoych@upc.edu.cn (Y. Cao).

https://doi.org/10.1016/j.gca.2019.01.001

inorganic reactions into geochemical models will improve the prediction of the evolution of organic and inorganic species in petroleum reservoirs.

Keywords: Oil-water-mineral systems; Organic-inorganic interactions; Mineral alteration; Oil degradation; Pathways; Ion exchange; Thermal experiments

1. INTRODUCTION

Over the last four decades, advances in the study of oil degradation (Aitken et al., 2004; Head et al., 2003; Hill et al., 2003; Jones et al., 2008; Tian et al., 2006; Waples, 2000) and water-rock interactions (Glasmann et al., 1989; Yuan et al., 2018, 2017; Zhu et al., 2010) based on laboratory experiments and natural reservoirs have improved our understanding of the respective reaction pathways of oil degradation and rock diagenesis in petroleum systems (Helgeson et al., 1993; Price, 1993; Seewald, 2003; van Berk et al., 2013; Zhang et al., 2012). Nevertheless, the scientific debate over whether chemical diagenesis occurs in oil-filled sandstones is still alive (Molenaar et al., 2008; Marchand et al., 2001; Worden et al., 2017). Additionally, the impact of some main mineral alterations (e.g., feldspar dissolution and relevant mineral precipitation, carbonate dissolution and cementation) on oil degradation in subsurface reservoirs has rarely been studied in detail (Seewald, 2001; van Berk et al., 2013). As elevated temperature and pressure increase the mutual solubility of oil and water, organic-inorganic interactions in subsurface oil-water-rock systems are expected to play an important role in the ongoing evolution of petroleum and rock quality (Lewan, 1997; Seewald, 2001, 2003; van Berk et al., 2013; Yuan et al., 2018). Hence, studies based on coupled mineral alteration and oil degradation in various thermal oil-water-mineral systems are necessary for deciphering the occurrence, pathways, and mechanisms of possible organic-inorganic interactions in hot hydrocarbon reservoirs.

Thermal experiment simulation is an essential and significant method to investigate oil degradation (Bu et al., 2017; Hill et al., 2003; Tian et al., 2010; Zhang et al., 2008) and water-rock interactions (Tutolo et al., 2015; Zhu and Lu, 2009). Oil cracking schemes and the relevant kinetics under anhydrous conditions have been studied extensively using numerous anhydrous pyrolysis experiments (Hill et al., 2003; Pan et al., 2010; Tian et al., 2006; Tsuzuki et al., 1999; Waples, 2000). However, few studies have been conducted to investigate the pathways and relevant kinetics of oil degradation and mineral evolution in hydrous hydrocarbon-water-mineral systems. Seewald (2001, 2003) proposed a stepwise oxidation mechanism for the decomposition of low-molecular hydrocarbons to form methane-rich gas in hot hydrocarbon-water-iron mineral systems with a high water/hydrocarbon ratio. The promoting or inhibiting effects of water, certain minerals (illite, montmorillonite, calcite, quartz), and salts ($MgSO_4$, NaCl, Na_2SO_4) on oil degradation have been investigated in some previous studies using liquid and gaseous hydrocarbon data from pyrolysis experiments with geochemical systems of oil plus water, oil plus minerals, or oil plus water plus minerals (salts) (Pan et al., 2010; Wang et al., 2015; Xiao et al., 2010; Zhang et al., 2008). In hot oil-water-mineral systems, the chemical composition evolutions of the pore water and gases, as well as mineralogical data, are all mandatory for elucidating how the organic oil degradation and inorganic mineral alteration reactions are coupled and interact with each other in the systems with various compositions. However, the ions and organic acids in the water after the completion of complex interactions and mineral alteration processes in these experiments have rarely been analyzed and few attempts have been made to couple the complex organic and inorganic processes (Seewald, 2001; van Berk et al., 2013).

Feldspar diagenesis is ubiquitous and significant in arkose reservoirs prior to and after oil charging (van Berk et al., 2013; Molenaar et al., 2015; Yuan et al., 2018, 2015a). However, the interactions between feldspar minerals and oil degradation products in natural deep reservoirs have rarely been explored. Our study is based on the results of two sets of experiments with different oil-deionized (or 0.5 mol/L NaCl) water-feldspar systems heated to 360 °C (Fig. 1). One set of the experiments was conducted for two days and the other for six days. The kinetics of oil degradation (Waples, 2000) and mineral alteration (Palandri and Kharaka, 2004) suggest that the heating experiments at 360 °C for two and six days may produce results similar to subsurface petroleum reservoirs heated at 160 °C for approximately 5000 years and 15000 years and indicate the generation of various and significant mineral alteration and oil degradation reactions. In addition, the 360 °C temperature of the experiments is lower than the critical temperature of water (374 °C for deionized water and higher for saline water) (Haas, 1976; Lewan, 1997), and supercritical water is avoided in the present experiments. Because oil comprises various components, pyrolysis experiments of single eicosane ($C_{20}H_{42}$) in hydrous and anhydours systems were also conducted for six days at 360 °C to facilitate the discussion of hydrocarbon degradation (Fig. 1). For the first time, we performed an integrated and quantitative analysis of the changes in the minerals, water compositions, hydrocarbons, CO_2, H_2, and organic acids in these experiments. Our results suggest that water can remarkably promote oil degradation and that the mineral alteration and the oil degradation interact and affect each other significantly, with water serving as a matrix for the potential exchange of H^+ and OH^-. The organic-inorganic interactions proceed along different pathways in different geochemical environments. The incorporation of such organic-inorganic interactions and detailed geological parameters including petrography and water chemistry into geochemical models is needed for improving

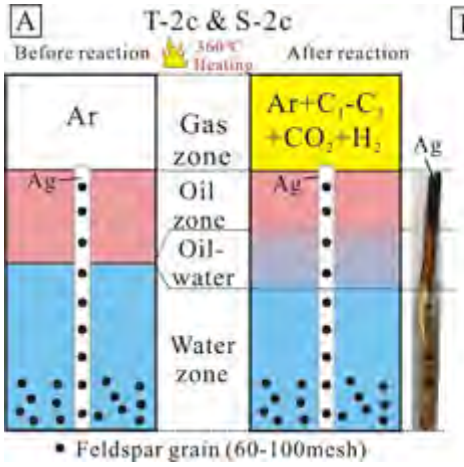

B

T- set 2-day	S-set 6-day	Oil (g)	D-water (g)	NaCl water (g)	Feldspar
T-1a	S-1a	2±0.05	/	/	7-9 grains
T-1b	S-1b	2±0.05	/	/	1.0 g
T-2a	S-2a	2±0.05	5±0.05	/	/
T-2b	S-2b	2±0.05	5±0.05	/	7-9grains
T-2c	S-2c	2±0.05	5±0.05	/	1.0 g
T-3	S-3	/	5±0.05	/	1.0 g
T-4a	S-4a	2±0.05	/	5±0.05	/
T-4b	S-4b	2±0.05	/	5±0.05	7-9 grains
T-4c	S-4c	2±0.05	/	5±0.05	1.0 g
T-5	S-5	/	/	5±0.05	1.0 g
/	S-6a	2g $C_{20}H_{42}$	/	/	/
/	S-6b	2g $C_{20}H_{42}$	5±0.05	/	/

Fig. 1. Detailed design of the two sets (2-day and 6-day) of oil (eicosane)-water-rock experiments. (A) Images showing the distribution of oil, water, feldspar grains, and silver (Ag) bar in the T-2c and S-2c experiments. The silver bar was cleaned with acetone to remove the liquid oil after the experiment; the color of the silver bar in the S-2c experiment after 6-day heating represents the distribution of pyrobitumen (black) in different zones. (B) Detailed oil (eicosane)-water-feldspar compositions of the twenty two experiments. The detailed composition of the feldspar used in the experiments is shown in Table 1.

the prediction of the occurrence of hydrocarbons, water, and rock properties in natural reservoirs.

2. SAMPLES AND METHODS

2.1. Sample preparation

Crude oil in the Lower Eocene sandstone reservoirs was collected from well Yan22-X95 at the depth of approximately 3500 m in the Minfeng area of the Dongying Sag, Bohai Bay Basin, East China. The temperature of the oil reservoirs is lower than 135 °C and a geothermal gradient of approximately 34 °C/km exists. The details of the geological setting of the Dongying Sag are available in previous studies (Guo et al., 2010; Li et al., 2010; Ma et al., 2017; Ping et al., 2010; Song et al., 2009). The crude oil is composed of 81.2% saturates, 8.4% aromatics, 6.8% resins and 3.6% asphaltenes. The Gas Chromatogram of the whole crude oil is presented in Fig. 9A. The detailed information on the aromatics based on a Gas Chromatogram–Mass Spectrometry (GC–MS) analysis are presented in Fig. A1 and Table A1. Aside from the main saturated hydrocarbons, unsaturated hydrocarbons including various benzenes, cyclohexane, naphthalines, phenanthrene, fluorine, sulfur-containing components including various dibenzothiophenes, thiophenes, and oxygen-containing components including dibenzofurans were detected in the crude oil (Fig. A1, Table A1). The eicosane sample used in the experiments was produced by the Aladdin Industrial Corporation and had a purity greater than 99.5%. A NaCl solution with a concentration of 0.5 mol/L was prepared with 99.99% NaCl and deionized water (D water). The orthoclase crystals consisting mainly of K-feldspars (Table 1) were ground with an agate mortar and pestle and subsequently dry sieved to retain a size fraction between 150 μm (100 mesh) and 250 μm (60 mesh). An additional 100 K-feldspar grains with a size of approximately 0.5–1 mm were selected separately. The feldspar grains were ultrasonically cleaned with analytical-grade acetone and D water three times to remove the submicron-to-micron sized particles adhering to the feldspar surface. The feldspar grains were then dried at 60 °C and analyzed with a Coxem-30 plus scanning electron microscope (SEM) to ensure the total removal of the small particles. Ten silver bars (2.5 mm diameter, 80–90 mm in length) were prepared and 7–9 holes (0.5–1 mm diameter)

Table 1
Detailed elemental composition of the mineral sample used in the experiments. The major elements and trace elements with content higher than 1 μg/g are listed.

Component	Content, %	Component	Content, μg/g	Component	Content, μg/g
SiO_2	66.70	Cl	485	V	7.79
Al_2O_3	17.97	Rb	402	Ce	14.6
Fe_2O_3	0.214	Sr	192	La	8.25
MgO	0.104	Ba	2131	Nd	6.97
CaO	0.557	Cu	17	Pb	32.5
Na_2O	1.580	Zn	13.3	Y	4.95
K_2O	11.94	Ga	20.6	Zr	13.1
MnO	0.007	Ni	3.82	Th	2.91
TiO_2	0.079	Li	7.54	Cs	2.85
P_2O_5	0.016	Be	3.7	Pr	1.8
SO_2	0.002	Cr	3.15	Sm	1.31

were drilled into the bars using a micro-drill. The big feldspar grains were placed into these holes for the purpose of identifying the mineral evolution features in the oil, oil-water, and water zones in the hot oil-water-feldspar systems. The silver bars with the feldspar were cleaned with acetone and D water and then dried at 60 °C.

2.2. Thermal simulation experiments

The high-temperature thermal simulation experiments were conducted at the State Key Laboratory of Organic Geochemistry of the Guangzhou Institute of Geochemistry. Hastelloy pressure reactors (20 mm outside diameter, 5 mm wall thickness, and 120 mm height) were used for the two sets (2-day and 6-day) of thermal experiments (Fig. 1A). All reactors were heated to 750 °C for 8 h to burn any remaining organic matter. After heating, the reactors were cleaned with acetone and D water and were dried at 60 °C. The oil, water, feldspar, and silver bars with the mineral grains with different combinations were placed into the ten Hastelloy pressure reactors for each set of experiments. The detailed compositions of the oil, water, and feldspars of the twenty experiments are listed in Fig. 1B. The pyrolysis of the eicosane ($C_{20}H_{42}$) was also conducted in the Hastelloy pressure reactors at 360 °C, with 2 g eicosane in the anhydrous system, 2 g eicosane plus 5 g D water in the hydrous system (Fig. 1B). Once loaded, the open ends of the reactors were purged with argon to remove air from the reactor; subsequently, the reactors were sealed in the presence of argon. Lastly, all reactors with the samples were weighed.

For each set of experiments, the reactors were placed in a single furnace with a fan at the bottom to keep the vessels at the same temperature during the experiment. The thermal experiments were conducted at 360 °C and the temperature was controlled by a thermocouple placed in the furnace and attached to one of the reactors. The error of the temperature measurements was $<\pm 1$ °C (Bu et al., 2017). The initial heating of the reactors to 360 °C was achieved in approximately 12 h, and the subsequent isothermal heating period lasted for 48 h (2 days) for the first set of experiments (T-set in Fig. 1B) and 144 h (6 days) for the other set (S-set in Fig. 1B). After heating, the reactors were quenched to room temperature in cold water within 10 min. After drying at room temperature, the reactors were weighed again to ensure that no materials had escaped from the reactors during the heating processes.

2.3. Analysis of gases, liquids, and minerals

The crude oil sample were treated with *n*-hexane to precipitate the asphaltene fractions. The resultant fractions were further fractionated into saturated hydrocarbon, aromatic hydrocarbon, and resin fractions by column chromatography using activated silica gel/alumina (3:2, w/w). The saturated and aromatic hydrocarbons were eluted with *n*-hexane and a mixture of dichloromethane/*n*-hexane (2:1, v/v), respectively. GC–MS analyses of the saturated hydrocarbon fractions were conducted using on an Agilent 5975C mass spectrometer coupled to an Agilent 6890 N gas chromatograph equipped with an DB5-MS capillary column (60 m × 0.25 mm × 0.25 μm film thickness). The mass spectrometer was operated in both full-scan and selected ion monitoring (SIM) modes with an electron ionization mode at 70 eV. The GC oven temperature was initially set at 60 °C with a holding time of 1 min and was programmed to reach 120 °C at 20 °C/min and then 310 °C at 3 °C/min with a final holding time of 25 min. The aromatic hydrocarbon fractions were analyzed using the same equipment and column but with a different temperature program (Cheng et al., 2018). For the analyses of the aromatic fractions, the GC oven temperature was initially set at 60 °C for 1 min and programmed to reach 310 °C at 3 °C/min with a final holding time of 16 min. The mass spectrometer was operated in the full scan mode with an electron ionization mode at 70 eV. Helium was used as the carrier gas.

After heating, the volatile components in the reactors were collected in a special sampling device connected to an Agilent 6890N gas chromatograph modified by Wasson-ECE Instrumentation as described previously (Bu et al., 2017; Pan et al., 2012; Tian et al., 2006). Briefly, the whole device was at first evacuated to $<1 \times 10^{-2}$ Pa. The reactor was then opened in the vacuum device, allowing the gases to escape into the device. The valve connecting the device and the modified gas chromatograph was open to allow the gas components to enter the gas chromatograph; in this manner, the GC analyses of the organic and inorganic gas components were performed using an automatically controlled procedure. The oven temperature for the hydrocarbon gas analysis was initially held at 70 °C for 6 min, ramped from 70 to 130 °C at 15 °C/min, from 130 to 180 °C at 25 °C/min, and was then held at 180 °C for 4 min, whereas it was held at 90 °C for the inorganic gas analysis. The analysis of all gases was carried out with a single injection. A test with external standard gases indicated that the amounts of the gas products measured using this device had a relative error of <0.5%.

After the GC analysis, some of the remaining gas components trapped within the device were used for GC-isotope ratio mass spectrometry (GC-IRMS) using a 10 ml syringe to pierce the septum of the device (Bu et al., 2017; Pan et al., 2012; Tian et al., 2006). This analysis was performed on a VG Isochrom II interfaced to an HP 5890 GC. The HP 5890 GC was fitted with a Poraplot Q column (30 mm × 0.32 mm i.d.). Helium was used as the carrier gas. The column head pressure was 8.5 psi. The gas chromatograph oven temperature was initially held at 40 °C for 3 min, ramped from 40 to 180 °C at 20 °C/min, and held at 180 °C for 5 min. The carbon isotopic value of the CO_2 reference gas was calibrated by NBS-22 oil as a reference material using elemental analysis (Thermo Quest Flash EA 1112 Series), combined with the isotope ratio mass spectrum (Delta Plus XL). The carbon isotope ratios for the individual gaseous hydrocarbons were calculated using CO_2 as a reference gas that was automatically introduced into the IRMS at the beginning and end of each analysis. In addition, a standard mixture of gaseous hydrocarbons (C_1–C_4) with known isotope compositions calibrated by our laboratory, was used daily to test the performance of the instrument. The standard deviation for the replicate analyses of this mixture is <0.3‰ for each compound.

After analysis of the gas components, the light hydrocarbons (C_6–C_{10}) were collected in a vial by liquid nitrogen freezing and the liquid hydrocarbon components remaining in the reactor and 3 ml pentane were extracted by a syringe into a vial. Two internal standards of deuterated *n*-C_{22} and *n*-C_{24}, ranging from 0.048 to 0.063 mg and 0.049 to 0.065 mg, respectively, were added to each vial. Following five ultrasonic treatments of 5 min per treatment, these vials were allowed to settle for 72 h until the pentane solutions became clear. The pentane solutions (total pentane extracts) in all the vials were directly injected into the HP6890 gas chromatograph fitted with a 30 mm × 0.32 mm i.d. column coated with a 0.25-mm film of HP-5, employing nitrogen as a carrier gas. The oven temperature was programmed as follows: 50 °C for 5 min, raised from 50 to 150 °C at 2 °C / min, and from 150 to 290 °C at 4 °C /min, and then held at 290 °C for 15 min.

The residual oil-water solutions after the oil extraction were then filtered with C_{18} molecular sieves to obtain the water samples. Each of the water samples was divided into two parts. One part was tested using an EGC automatic leaching device, an Ion Pac ASl5 separation column (4 mm × 250 mm), an Ion-Pac AGl5 guard column (4 mm × 50 mm) and an ICS-900 Ion Chromatograph to obtain the concentration of the organic acids, Cl^- and SO_4^{2-}, with an error <0.01%; the analysis was performed in the State Key Laboratory of Organic Geochemistry of the Guangzhou Institute of Geochemistry. The other part was tested using an ICP-MS (Thermo icapQ, USA) to obtain the concentration of the cations including Al, Si, K, Na, and Ca, with an error of <0.001 ppm; the analysis was conducted at the Analytical and Measurement Research Center of the Qingdao Institute of Oceanology.

The composition of the minerals used in the present experiments was determined by an Axios mAX X-ray fluorescence spectrometer and the trace elements were determined by an ELEMENT XR ICP-MS in the CNNC Beijing Research Institute of Uranium Geology. After the thermal experiments, the silver bars and feldspars grains were firstly cleaned using acetone and D water to remove the oil covering the mineral surface. The cleaned mineral grains and silver bar with the minerals were then fixed on aluminum stubs with conducting tape and were coated with gold. The treated minerals were then identified using the Coxem-30plus SEM to describe the textures of the feldspars and secondary minerals. A Bruker energy dispersive spectrometer (EDS) system (XFlasher Detector 430-M), which allows for the analysis at a specific spot of about 1 μm diameter was used to test the chemical composition of the minerals with an error of 0.1%.

3. RESULTS

3.1. Leached feldspars and secondary minerals in various systems

The SEM images show that the fresh surfaces of the feldspar grains prior to the experiments are relatively flat and no typical leaching pits on the feldspar surfaces, leaching intergranular pores in the feldspar grains, or euhedral secondary minerals can be identified (Fig. 2A). In contrast, after the reactions, different minerals developed in different systems and exhibit various textures (Figs. 2–5).

In the anhydrous oil-feldspar systems (T/S-1a, T/S-1b), only very few small pits occur on some feldspar grains (Fig. 2B and C) in the oil-feldspar systems after heating for 2–6 days. No secondary minerals were identified on the feldspar surfaces. In the D water-feldspar systems, K-feldspars were leached extensively (Fig. 2E) to form amorphous minerals and some kaolinite after the 2-day reaction (T-3) and illite and muscovite after the 6-day reaction (S-3). In the NaCl water-feldspar system, K-feldspar was leached extensively (Fig. 2G and L) to form thin plate paragonite minerals after the 2-day reaction (T-5) and authigenic albite minerals after the 6-day reaction (S-5).

In the oil-D water-few feldspar systems, feldspar minerals were leached extensively after the two-day (Fig. 2D) and six-day (Fig. 2H) experiments. After two days (T-2b), the secondary minerals formed in the water, water-oil, and oil zones are euhedral lash-shaped boehmite (y-AlO(OH)) with a length of 4–8 μm, subhedral lash-shaped boehmite with a length of 1–2 μm, and fibrous illite, respectively (Fig. 3A). After six days (S-2b), these minerals evolve to flower-like muscovite aggregates in the water zone, flower-like muscovite aggregates and subhedral thin muscovite plates in the water-oil zone, and euhedral octahedral muscovite plates in the oil zone (Fig. 3A), respectively. In the oil-NaCl water- few feldspar system, the feldspar minerals were also leached extensively after the two-day (Fig. 2F) and six-day (Fig. 2J) experiments. After two days (T-4b), the secondary minerals formed within two days (T-6) in the water, water-oil, and oil zones are euhedral lash-shaped boehmite with a length up to 50 μm, euhedral-subhedral lash-shaped boehmite with a length of 10–30 μm, and a combination of grouped filament-like boehmite and thin paragonite ($NaAl_2[AlSi_3O_{10}(OH)_2]$) plates surrounding the boehmite, respectively (Figs. 4A; 5C). After six days (S-4b), these minerals evolve into honeycomb-like paragonite aggregates in the water zone, with additional subhedral thin paragonite plates in the water–oil zone and additional small columnar albite in the oil zone (Fig. 4A). In the oil-water-feldspar systems with a high mineral/fluid ratio (T/S-2c, T/S-4c), the feldspar dissolution is also extensive (Fig. 2I and K). However, after 2-day and 6-day heating, boehmite was not identified but illite and muscovite (Fig. 5A and B) were present in the oil-D water-feldspar system (T/S-2c); paragonite and albite (Fig. 5D–F) were identified in the oil-NaCl water-feldspar system (T/S-4c).

3.2. Gaseous components produced by the experiments

3.2.1. Yield of hydrocarbon gases, CO_2, and H_2

The amounts of gaseous hydrocarbons (C_1–C_5), CO_2, and H_2 produced from the crude oil degradation are shown in Fig. 6A and B (detailed data are shown in Table 2). The results show that the 6-day experiments generated more hydrocarbon gases than the 2-day experiments under the same conditions. The amounts of methane are the highest (0.61–2.90 ml/g oil in 2-day, 3.29–6.35 ml/g oil in 6-day) in all the experiments with oil, followed by ethane and pro-

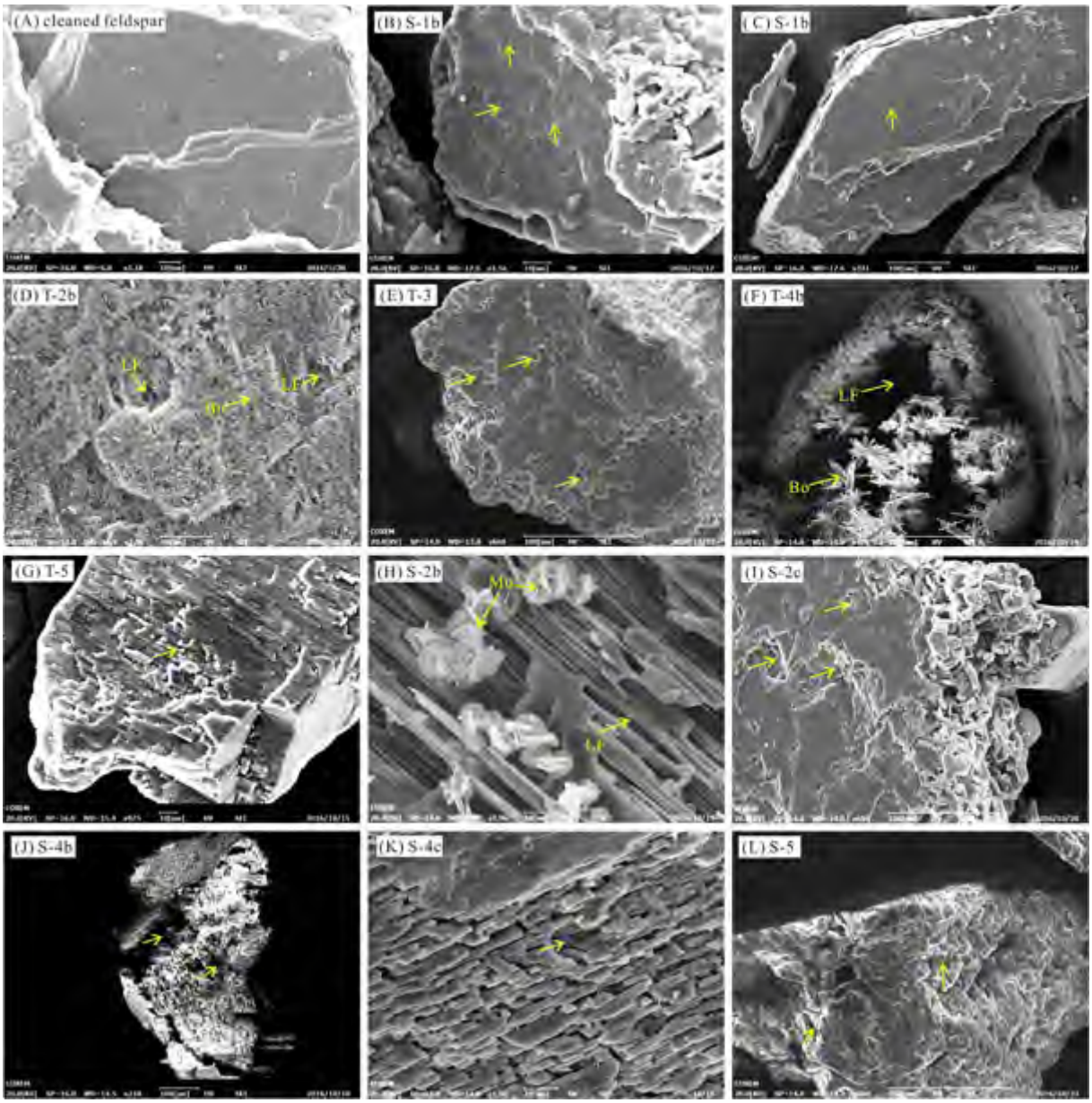

Fig. 2. SEM images of feldspars prior to experiments, leached feldspars, and authigenic minerals in some experiments. (A) Surface of K-feldspar grains prior to the experiments; (B) small pits on the surface of K-feldspar in the oil-feldspar system (S-1b) after 6-day heating; (C) K-feldspar grain with limited alteration in the oil-feldspar system (S-1b) after 6-day heating; (D) extensively leached K-feldspar (LF) and euhedral boehmite crystals (Bo) in the oil-water zone of the oil-D water-few feldspar system (T-2b) after 2-day heating, enlargement of boehmite is shown in Fig. 3A; (E) extensively leached K-feldspar surface in the D-water-feldspar system (T-3) after 2-day heating; (F) extensively leached K-feldspars and euhedral boehmite in the water zone of the oil-NaCl water-few feldspar system (T-4b) after 2-day heating; (G) extensively leached K-feldspars in the NaCl water- feldspar system after 2-day heating; (H) extensively leached K-feldspars and euhedral muscovite (Mu) in the water zone of the oil-D water-few feldspar system (S-2b) after 6-day heating; (I) extensively K-feldspar dissolution in the oil-D water-feldspar system (S-2c) after 6-day heating; (J) extensive K-feldspar dissolution in the oil zone of the oil-NaCl water-few feldspar system after 6-day heating; (K) extensively leached K-feldspar in the oil-water zone of the oil-NaCl-few feldspar system (S-4c) after 6-day heating; (L) extensive K-feldspar dissolution in the NaCl water-few feldspar system after 6-day heating.

pane (0.22–1.68 ml/g oil in 2-day, 0.77–4.38 ml/g oil in 6-day) at the same magnitude. The amounts of butane (0.12–0.67 ml/g oil in 2-day, 0.30–2.03 ml/g oil in 6-day) and pentane (0.04–0.27 ml/g oil in 2-day, 0.10–0.73 ml/g oil in 6-day) are much lower than those of the C_1–C_3 alkanes, with the amount of i-C_4 lower than n-C_4 but i-C_5 higher than n-C_5. The olefins including ethene and propene are gaseous hydrocarbons with the lowest amounts (0.01–0.05 ml/g oil in the 2-day and 0.01–0.07 ml/g oil in 6-day). For the non-hydrocarbon gases, the amounts of CO_2 released from the heated oil range from 0.03 ml/g to 0.24 ml/g oil after 2-day heating and 0.02–0.22 ml/g after

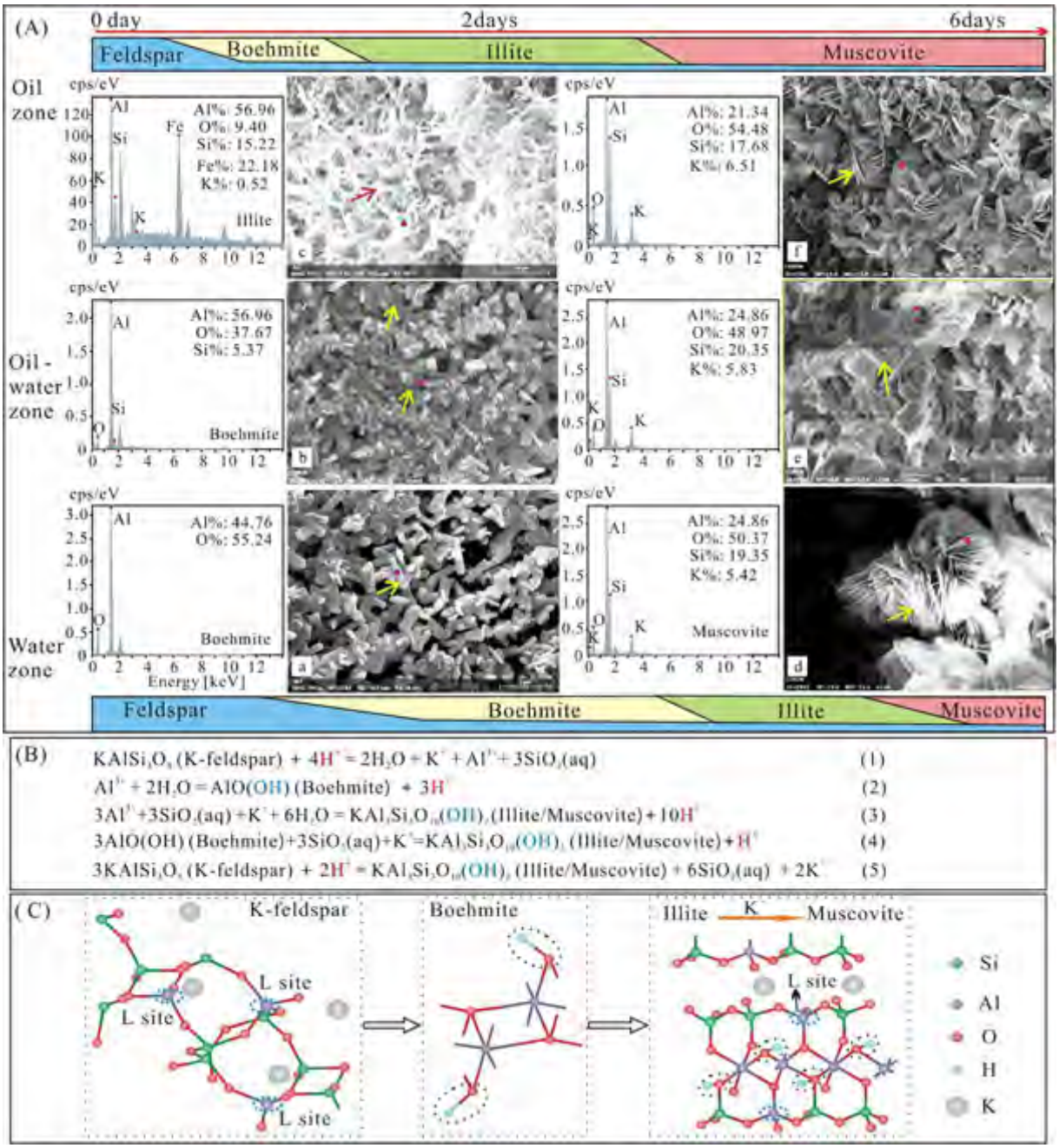

Fig. 3. Mineral evolution and relevant chemical reactions in the 2-day and 6-day experiments in the oil- D water-few feldspar grain systems with a low mineral/water ratio (T/S-2b). (A) Scanning electron microscope (SEM) and Energy Disperse Spectroscopy (EDS) evidence for the mineral evolution in the oil, oil-water, and water zones after 2-day (T-2b) and 6-day (S-2b) reactions, a: euhedral boehmite, b: subhedral boehmite, c: fibrous illite, d–f: muscovites with different textures; (B) chemical reactions involved in the mineral alteration from K-feldspar to illite/muscovite (Yuan et al., 2017; Zhu et al., 2010). Note that H^+ is involved in all the reactions; H^+ may originate from CO_2, organic acids, and water; (C) crystal structures of K-feldspar (Yang et al., 2013), boehmite (Raybaud et al., 2001), illite and muscovite (Hu et al., 2003). OH^- is present in all the secondary minerals including boehmite, illite and muscovite; from illite to muscovite, more K^+ is introduced into the interlayer space. L site denotes the Lewis acid site in the aluminosilicate minerals.

6-day heating. The amounts of H_2 are much higher than those of the CO_2, and range from 0.11 to 0.50 ml/g oil in the 2-day experiments and 0.34–0.60 ml/g oil in the 6-day experiments. From two days to six days, the amounts of CO_2 and H_2 do not increase much, except for the H_2 in the anhydrous systems (T/S-1a, T/S-1b). In both the 2-day and 6-day experiments, the hydrous systems generate much more hydrocarbon gases and CO_2 than the anhydrous experiments (Fig. 6A and B). Additionally, the oil-NaCl water system generates even more gases than the

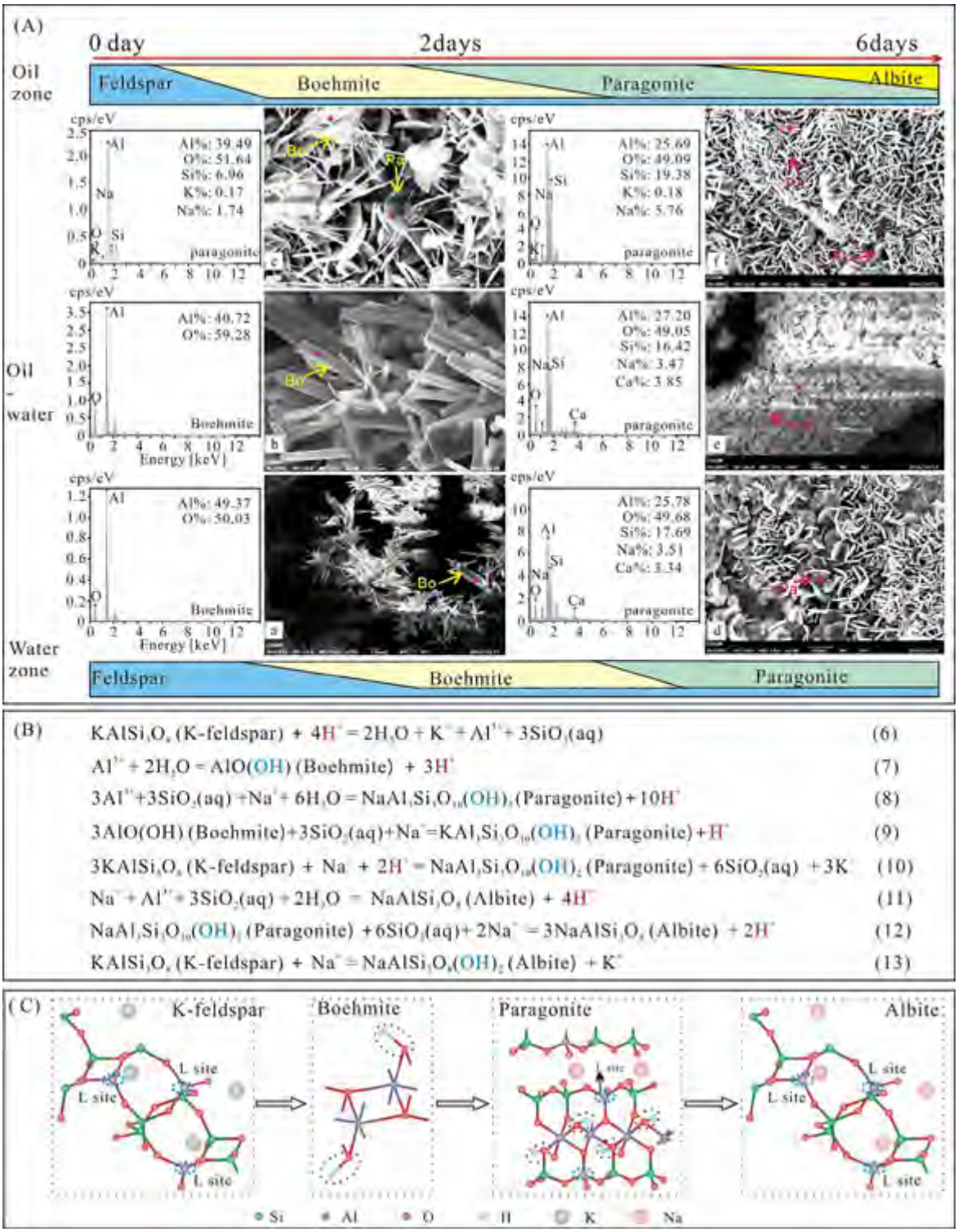

Fig. 4. Mineral evolution and relevant chemical reactions in the 2-day and 6-day experiments in the oil-NaCl water-few feldspar grain systems with a low mineral/water ratio (T/S-4b). (A) SEM and EDS evidence for the mineral evolution at different zones after 2-day and 6-day reactions, a: euhedral boehmite, b: euhedral-subhedral boehmite, c: boehmite (Bo) and paragonite (Pa), d–f: paragonite with different textures and euhedral albite (Al); (B) chemical reactions involved in the mineral alterations, H^+ is involved in all reactions except for the reaction from K-feldspar to albite (Lu et al., 2013); (C) crystal structures of K-feldspar and albite (Yang et al., 2013), boehmite (Raybaud et al., 2001), and paragonite (Brown and Nadeau, 1984; Deer et al., 2013). OH^- is present in both the boehmite and phyllosilicates including illite and muscovite but absent in the tectosilicate K-feldspar and albite. L site denotes the Lewis acid site in the aluminosilicate minerals. H^+ may originate from CO_2, organic acids and water.

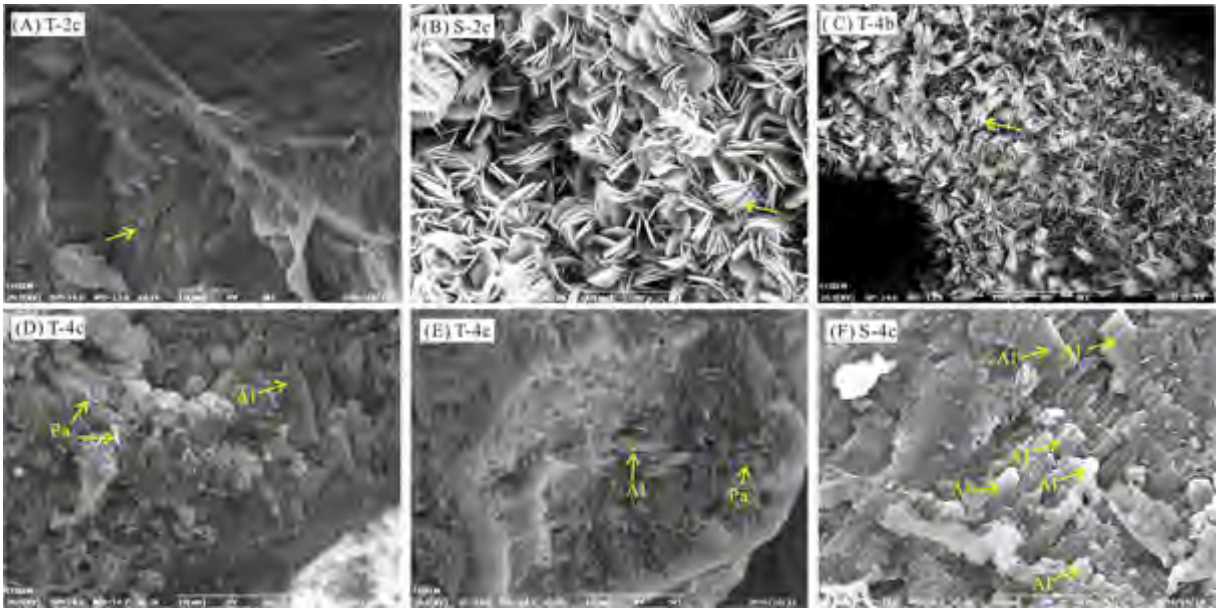

Fig. 5. SEM images of some secondary minerals in different experiments. (A) Illite on the feldspar surface in the oil zone of the oil-D water-feldspar system (T-2c) after 2-day heating; (B) muscovite in the oil zone of the oil- D water-feldspar system after 6-day heating; (C) boehmite formed in the oil zone of the oil-NaCl water-few feldspar system after 2-day heating; (D) paragonite (Pa) and albite (Al) in the oil zone of the oil-NaCl water-feldspar system (T-4c) after 2-day heating; (E) paragonite and albite in the water zone of the oil-NaCl water-feldspar system after 2-day heating; (F) albite formed in the oil zone of the oil-NaCl water-feldspar system (S-4c) after 6-day heating.

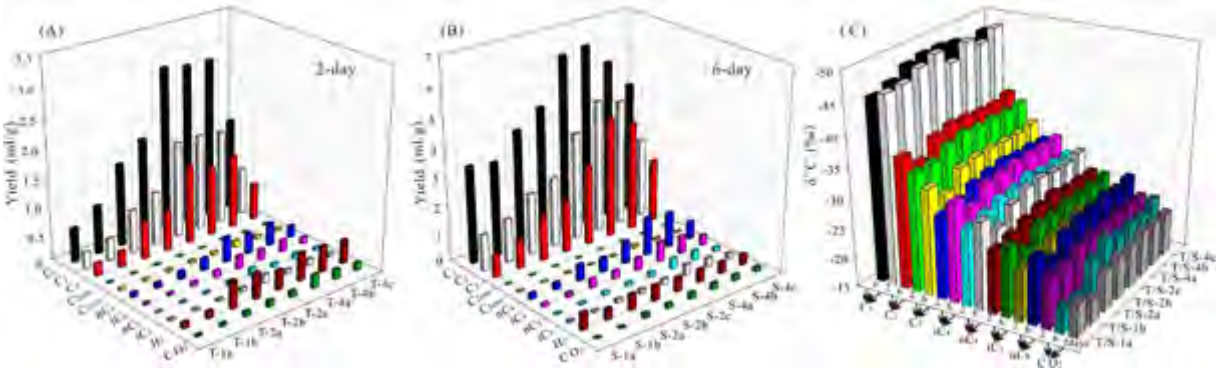

Fig. 6. Experimental data of alkane, alkene, H_2, and CO_2 in different experiments with crude oil. (A, B) Yield of C_1–C_5 alkanes, ethane (C_{2ene}), propylene (C_{3ene}), H_2 and CO_2 in the 2-day (A) and 6-day (B) experiments; (C) $\delta^{13}C$ values of CO_2 and C_1–C_5 gases. Detailed data are provided in Table 2.

oil-D water system. The amounts of H_2 are higher in the hydrous experiment than in the anhydrous system in the 2-day experiments, whereas the amounts of H_2 are nearly equivalent in all the 6-day experiments. With the addition of 1 g of feldspar, much more hydrocarbon gases were produced than in the system with oil and D water. In contrast, less hydrocarbon gas was produced when the feldspars were added to the system with oil and NaCl water.

The amounts of gaseous hydrocarbons (C_1–C_5), CO_2, and H_2 produced from the eicosane degradation in the anhydrous and hydrous systems are shown in Fig. 7A (detailed data are shown in Table 2). Similar to the crude oil, the hydrous system generates much more alkane hydrocarbon gases than the anhydrous experiments. The amounts of H_2 generated in the anhydrous and hydrous systems after 6-day heating are 0.37 ml/g eicosane and 0.63 ml/g eicosane, respectively. It is worth noting that CO_2 was not detected in the anhydrous system; in contrast, the amount of CO_2 is 0.08 ml/g eicosane in the presence of water.

3.2.2. $\delta^{13}C$ of different hydrocarbon gases and CO_2

Overall, the $\delta^{13}C$ compositions of the generated methane to propane (C_1–C_5 *n*-alkanes including *iso*-alkanes) in the experiments with crude oil or eicosane are lighter in the 6-day experiments than in the 2-day experiments (Figs. 6C, 7B and Table 2). The $\delta^{13}C$ compositions of the generated alkanes are lighter in the hydrous experiments

Table 2
Detailed data of the gas yield of C_1–C_5, H_2, and CO_2, ratios of gas yields, and $\delta^{13}C$ composition of different gases.

Gases		Series																	
		2-day								6-day									
		T-1a	T-1b	T-2a	T-2b	T-2c	T-4a	T-4b	T-4c	S-1a	S-1b	S-2a	S-2b	S-2c	S-4a	S-4b	S-4c	S-6a	S-6b
Yield (ml/g)	C_1	0.607	0.859	1.465	1.774	2.900	2.828	2.818	1.619	3.414	3.286	4.138	4.691	6.246	6.347	5.589	4.572	0.797	1.438
	C_2	0.293	0.390	0.752	0.924	1.683	1.684	1.633	0.817	1.270	1.522	2.141	2.415	3.736	4.419	4.381	2.759	1.371	2.060
	C_3	0.229	0.283	0.634	0.704	1.385	1.209	1.294	0.649	0.770	0.993	1.579	1.772	2.778	4.195	3.814	2.201	0.615	0.919
	C_{2ene}	0.015	0.014	0.016	0.014	0.009	0.030	0.009	0.013	0.008	0.011	0.008	0.004	0.003	0.011	0.008	0.003	0.034	0.011
	C_{3ene}	0.040	0.040	0.046	0.051	0.050	0.104	0.055	0.044	0.026	0.040	0.038	0.028	0.025	0.099	0.071	0.028	0.099	0.079
	nC_4	0.083	0.092	0.138	0.216	0.443	0.351	0.393	0.203	0.195	0.241	0.572	0.495	0.766	1.338	1.217	0.618	0.152	0.246
	iC_4	0.037	0.044	0.075	0.116	0.227	0.188	0.209	0.108	0.108	0.145	0.311	0.274	0.431	0.692	0.611	0.345	0.002	0.006
	nC_5	0.024	0.026	0.027	0.058	0.133	0.061	0.088	0.046	0.047	0.053	0.107	0.117	0.151	0.345	0.314	0.148	0.029	0.054
	iC_5	0.026	0.028	0.032	0.066	0.139	0.071	0.104	0.056	0.053	0.060	0.126	0.137	0.179	0.385	0.296	0.165	0.001	0.006
	H_2	0.105	0.125	0.478	0.458	0.344	0.498	0.461	0.415	0.605	0.383	0.554	0.537	0.490	0.456	0.415	0.368	0.366	0.633
	CO_2	0.028	0.048	0.087	0.103	0.105	0.236	0.171	0.134	0.017	0.028	0.165	0.156	0.207	0.217	0.198	0.160	0	0.076
Ratios	C_1/C_2	2.075	2.203	1.948	1.921	1.723	1.679	1.725	1.982	2.688	2.160	1.933	1.943	1.672	1.374	1.276	1.657	0.567	0.694
	C_2/C_3	1.278	1.377	1.186	1.312	1.215	1.393	1.262	1.259	1.649	1.532	1.356	1.362	1.345	1.01	1.149	1.254	1.968	2.077
	$C_1/(C_2+C_3)$	1.164	1.276	1.057	1.090	0.945	0.978	0.962	1.105	1.673	1.307	1.113	1.120	0.959	0.720	0.682	0.922	0.376	0.469
	iC_5/nC_5	1.080	1.062	1.164	1.147	1.042	1.167	1.181	1.218	1.127	1.126	1.174	1.171	1.182	1.117	0.943	1.114	0.046	0.111
	iC_4/nC_4	0.447	0.477	0.544	0.536	0.513	0.536	0.532	0.534	0.555	0.600	0.543	0.553	0.563	0.514	0.502	0.559	0.011	0.024
	$C_1/(C_1–C_5)$	0.449	0.484	0.459	0.452	0.416	0.433	0.427	0.455	0.579	0.518	0.459	0.472	0.436	0.352	0.343	0.422	0.257	0.298
	C_{3ene}/C_3	0.175	0.139	0.072	0.072	0.036	0.086	0.042	0.068	0.034	0.040	0.024	0.017	0.009	0.024	0.019	0.013	0.161	0.086
	C_{2ene}/C_2	0.052	0.036	0.021	0.015	0.006	0.018	0.005	0.015	0.006	0.007	0.004	0.002	0.001	0.002	0.002	0.001	0.025	0.005
$\delta^{13}C$	C_1	−46.4	−46.5	−47.8	−48.8	−46.2	−48.4	−47.0	−48.6	−45.4	−46.3	−47.8	−48.4	−48.4	−48.0	−46.9	−47.6	−56.5	−59.9
	C_2	−34.8	−34.8	−36.1	−36.7	−36.3	−36.2	−35.8	−36.1	−36.9	−34.5	−37.2	−37.8	−37.5	−37.2	−37.1	−37.6	−39.7	−40.6
	C_3	−29.0	−29.6	−30.8	−31.2	−31.4	−31.0	−30.9	−30.5	−32.8	−30.2	−33.0	−33.3	−33.1	−32.9	−32.7	−33.1	−34.9	−36.3
	iC_4	−28.0	−28.5	−29.2	−29.2	−29.8	−29.1	−28.9	−28.8	−31.7	−29.2	−31.3	−31.5	−31.6	−31.3	−31.2	−31.3	/	/
	nC_4	−25.6	−26.2	−26.8	−27.4	−27.8	−27.0	−26.9	−26.6	−29.6	−26.7	−29.0	−29.9	−30.0	−29.4	−29.2	−29.6	−31.2	−32.7
	iC_5	−23.7	−24.3	−25.1	−25.4	−26.0	−24.9	−24.8	−24.7	−26.7	−24.2	−26.6	−26.5	−26.7	−26.5	−26.4	−26.5	/	/
	nC_5	−23.4	−23.5	−24.4	−24.5	−24.6	−24.8	−24.5	−24.2	−26.1	−23.9	−26.4	−27.0	−26.9	−27.2	−26.6	−27.1	/	/
	CO_2	−20.5	−19.1	−21.7	−22.1	−22.0	−22.8	−22.5	−22.2	−19.2	−19.0	−23.0	−24.7	−23.5	−23.5	−23.0	−24.2	−33.7	−34.8

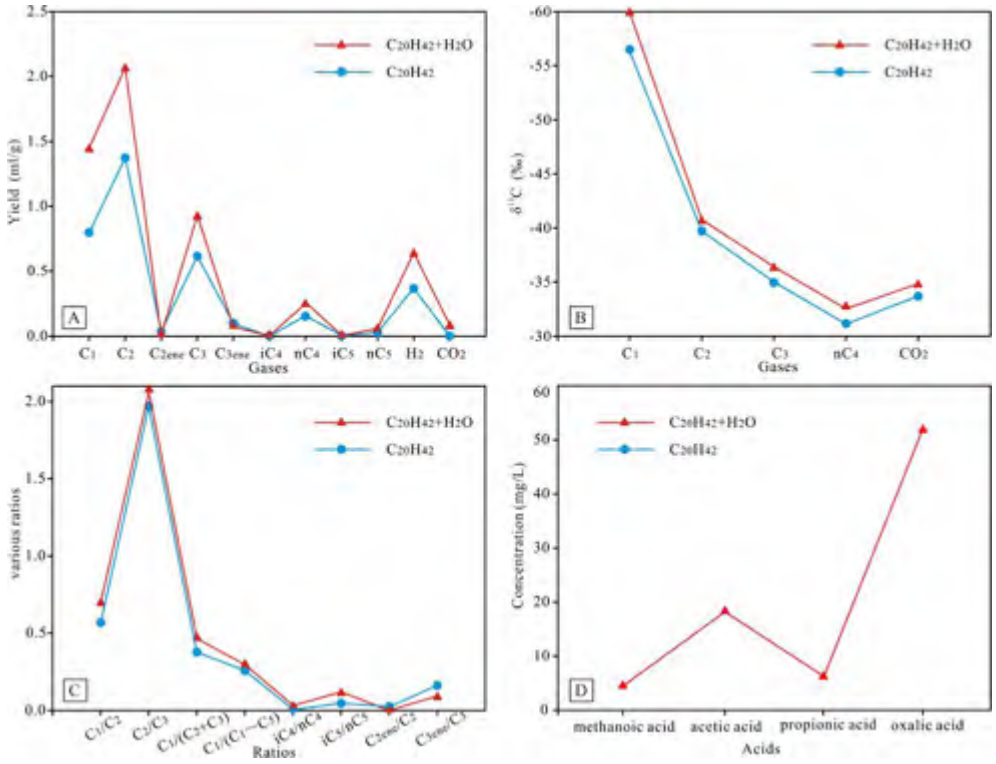

Fig. 7. Experimental data of alkanes, alkenes, H_2, CO_2, and organic acids in different experiments with eicosane. (A) Yield of C_1–C_5 alkanes, ethane (C_2ene), propylene (C_3ene), H_2 and CO_2 in the anhydrous and hydrous systems; (B) $\delta^{13}C$ values of CO_2 and C_1–C_4 gases; (C) ratios of different alkane/alkane, iso-alkanes/n-alkanes and alkene/alkane; (D) average concentrations of organic acids in the waters of the hydrous systems after the experiment. Detailed data are provided in Tables 2 and 3.

than in the anhydrous experiments, both in the 2-day and 6-day experiments. The $\delta^{13}C$ compositions of the CO_2 exhibit the same trend as the hydrocarbon gases and the differences are greater. The $\delta^{13}C$ data also show that the isotope differences between the systems with and without feldspars for specific gases are very small (Fig. 6C).

3.2.3. Ratios between different alkanes, ratios of alkenes/alkanes and iso-alkanes/n-alkanes

For the oil-containing experiments, the ratios of C_1/C_2, C_2/C_3, C_1/C_2+C_3, and C_1/C_1–C_5 are higher in the anhydrous experiments than in the hydrous experiments (Fig. 8A and Table 2). With the addition of 1 g of feldspar in T/S-2c, these ratios are lower than in T/S-2a and T/S-2b; whereas the addition of feldspar in T/S-4c makes these ratios higher than in T/S-4a and T/S-4b. In contrast, for the eicosane-containing experiments, the ratios of C_1/C_2, C_1/C_2+C_3, and C_1/C_1–C_5 are lower in the anhydrous experiments than in the hydrous experiments. The C_{2ene}/C_2 and C_{3ene}/C_3 ratios are much higher in the anhydrous system than in the hydrous system in both the eicosane-containing and the oil-containing experiments (Figs. 7C, 8B and Table 2). In the oil-containing systems, these ratios exhibit a decreasing trend with the addition of feldspars. From the 2-day to the 6-day experiments, these ratios decrease sharply in all experiments. The ratios of i-C_4/n-C_4 range from 0.45 to 0.55 and the ratios of i-C_5/n-C_5 range from 0.95 to 1.20 (Fig. 8A) in the oil-containing systems. For the 2-day experiments, the ratios are slightly higher in the hydrous experiments than in the anhydrous experiments, whereas no apparent difference is observed in the 6-day experiments. From the 2-day to the 6-day experiments, the i-alkane/n-alkane ratios in the systems without NaCl water change little, whereas the ratios in the systems with NaCl water decrease. With the addition of feldspars in the T/S-5 and T/S-8 systems, the ratios of i-alkanes/n-alkanes change little. For the eicosane-containing experiments, the ratios of i-C_4/n-C_4 and i-C_5/n-C_5 are extremely low, but still, the ratios are higher in the hydrous experiments than in the anhydrous experiments (Fig. 7C and Table 2).

3.3. Liquid oil components and pyrobitumen produced after the experiments

3.3.1. C_6–C_{33} components

The gas chromatograms show that the crude oil sample prior to the experiments consists of nC$_7$–nC$_{33}$, methylcyclohexane, toluene, and known biological precursors including pristane (Pr) and phytane (Ph) (Fig. 9A); the relative contents of the main components in the oil are represented by the dashed curves (Fig. 9). After the experiments, the differences in the gas chromatograms can be used to investigate the compositional change of the oil (Fig. 9B–I). For all the 2-day and 6-day experiments, the high-molecular alkanes (nC_{17}-nC_{33}), Pr, and Ph were degraded to form low-molecular alkanes (C_1–C_{12}), cyclopentane, methyl-cyclohexane, toluene, and xylene; the 6-day heating

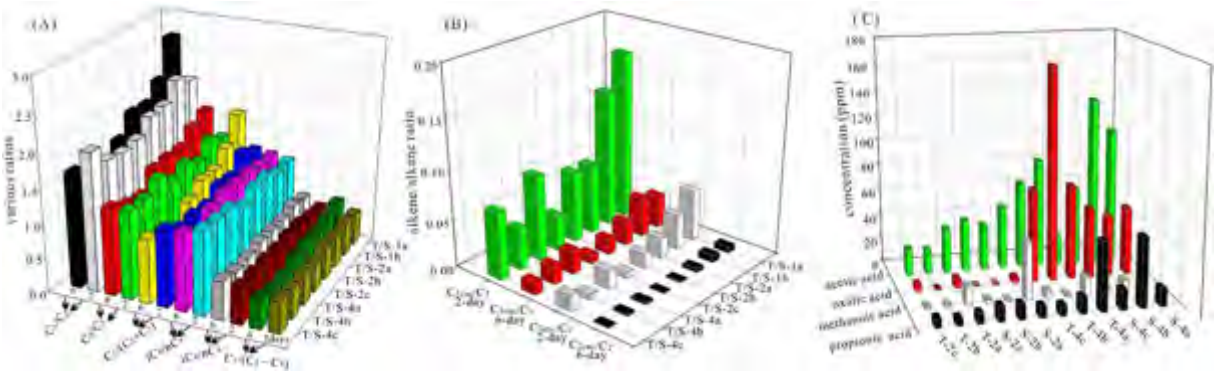

Fig. 8. Experimental data of the ratios of the yield of different alkanes and the ratios of *iso*-alkanes/*n*-alkanes (a), ratios of different alkene/alkane (b) and average concentrations of various organic acids in the waters after the experiments (c). Detailed data are provided in Tables 2 and 3.

degraded more high-molecular organics and some moderate-molecular organics.

In the hydrous systems with the D water and the NaCl water, more high-molecular organics were degraded to form low- molecular organics. Additionally, the system with the NaCl water degraded more high-molecular alkanes, Pr, and Ph than the system with D water (Fig. 9D and G). The oil-D water-feldspar system degraded more high-molecular materials and generated more C_{10}–C_{13} but less nC_6–C_9, cyclopentane, methyl-cyclohexane, toluene, and xylene than the oil-D water system (Fig. 9D–F). In contrast, the oil-NaCl-feldspar system degraded less high-molecular organic materials and generated less C_6–C_{13} (particular C_6–C_8), cyclopentane, methyl-cyclohexane, toluene, and xylene than the oil-NaCl system (Fig. 9G–I).

The gas chromatograms of the samples after the 6-day heating of the eicosane in the anhydrous and hydrous systems show that the eicosane was degraded to form large amount of C_6–C_{17}, small amounts of C_{18}, C_{19}, and also some $C_{>20}$ hydrocarbons (Fig. 10). A comparison of the two samples show that the hydrous system tend to generate more C_7–C_{11} but less C_{12}–C_{19}; in addition, the amounts of $nC_{>20}$ in the anhydrous system (Fig. 10A) are much higher than those in the hydrous system (Fig. 10B), even when the hydrous system degraded more eicosane and generated more C_1–C_5 gases (Fig. 7A).

3.3.2. Pyrobitumen produced by heating of the oil

After the experiments, the quantitative amount of pyrobitumen was not tested in each system. The presence of pyrobitumen on the mineral grain surfaces and the silver bars was identified for the purpose of analyzing its generation (Fig. 11). The SEM images show that the heavy oil and pyrobitumen attached to the feldspar surface is ubiquitous in the oil-feldspar system without water (Fig. 11A–D). In contrast, in the systems with oil, water, and minerals, the pyrobitumen can only be identified on the silver bar surface present in the pure oil zone (Figs. 11E and 1A) and little pyrobitumen adhered to the silver bars or the feldspar grain surfaces in the oil-water transitional zone or the water zone (Fig. 11F).

3.4. Ions in the experiments

3.4.1. Organic carboxylates produced after the experiments

The quantitative amounts of four types of carboxylates were tested in the oil-containing systems of T/S-2a, b, c and T/S-4a, b, c (Fig. 8C and Table 3). The data show that the organic acids in the oil-water-(mineral) systems in the experiments are dominated by acetic acid, followed by oxalic acid, propionic acid, and methanoic acid, which is consistent with the chemical data in pore waters from natural hydrocarbon reservoirs (Carothers and Kharaka, 1978; Surdam and Crossey, 1987). Except for the oxalic acid, the other three organic acids have higher concentrations in the 6-day experiments than in the 2-day experiments. The concentrations of the organic acids are lower in the systems with D-water than in the systems with NaCl water. The presence of feldspar in the system has no apparent impact on the concentration of the organic acids in the water. In the presence of water, the degradation of eicosane after 6 days also generates various carboxylates including 4.49 mg/L methanoic acid, 18.30 mg/L acetic acids, 51.82 mg/L oxalic acid, and 6.22 mg/L propionic acid.

3.4.2. Concentrations of cations and anions in the water after the experiments

The average concentrations of the various cations and anions in the water after the reaction are listed in Table 4. In the system with D water, the silicon has the highest concentration, followed by Cl^-, Na^+, and K^+; the concentrations of SO_4^{2-}, Ca^{2+}, and Al^{3+} are relatively low. The Na^+ and Cl^- concentration exhibit some differences in the systems with and without oil and the systems with the crude oil have higher concentrations of Cl^- and Na^+. After heating, the system with a low water/mineral ratio has higher concentrations of Si^{4+} and Ca^{2+} but a lower concentration of K^+. In the system with the NaCl water, the concentrations of Cl^- and Na^+ are much higher than for the other solutes, followed by K^+, Si^{4+}, SO_4^{2-}, and Al^{3+}. After heating, the system with a lower water/mineral ratio has higher concentrations of Si^{4+}, K^+, and Ca^{2+} but a lower concentration of Al^{3+}. The presence of high concentrations of

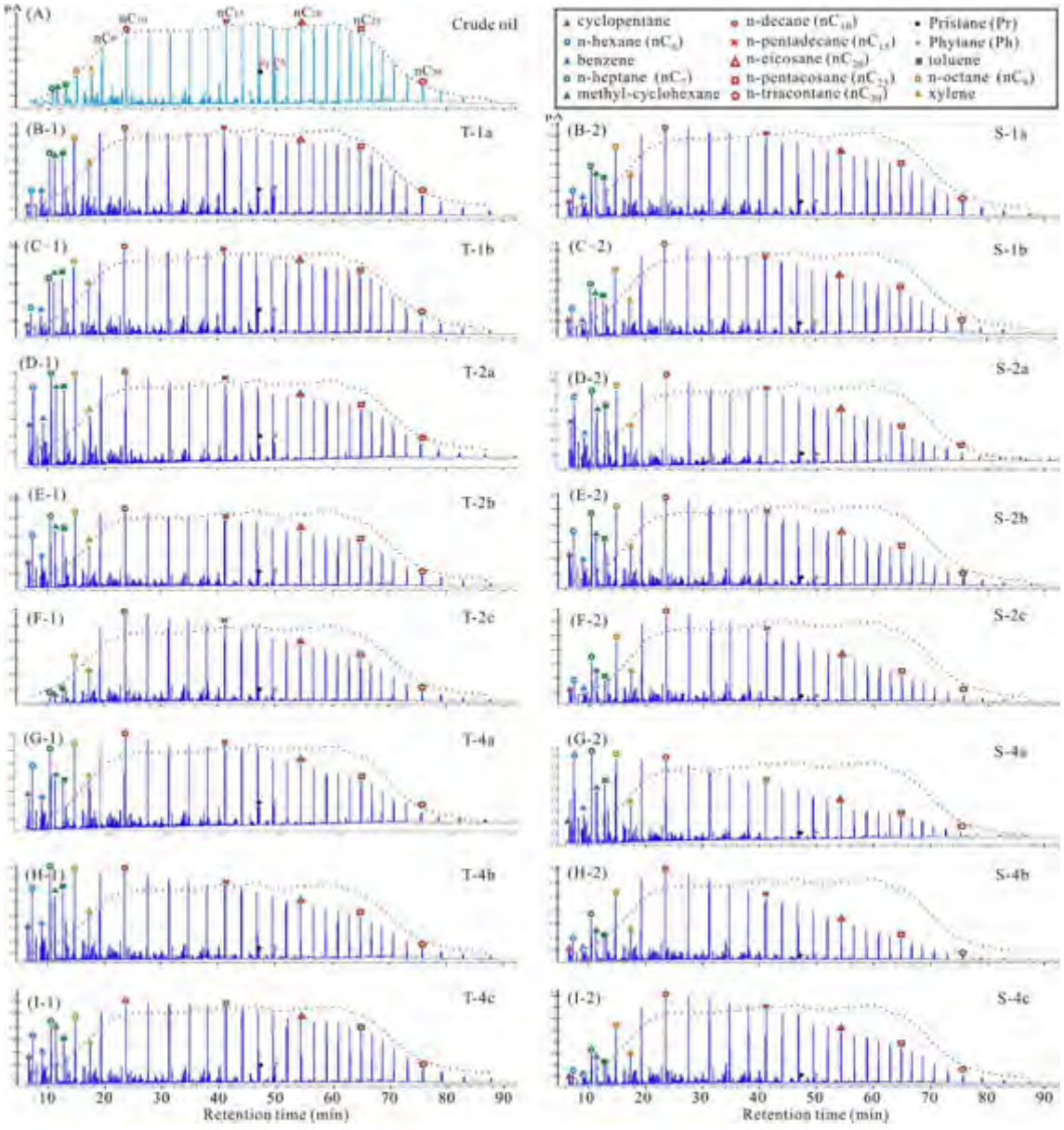

Fig. 9. Gas chromatograms of the oil samples prior to (a) and after the experiments (b–g). The dashed curves represent the pattern of main compositions in the crude oil sample prior to the experiment.

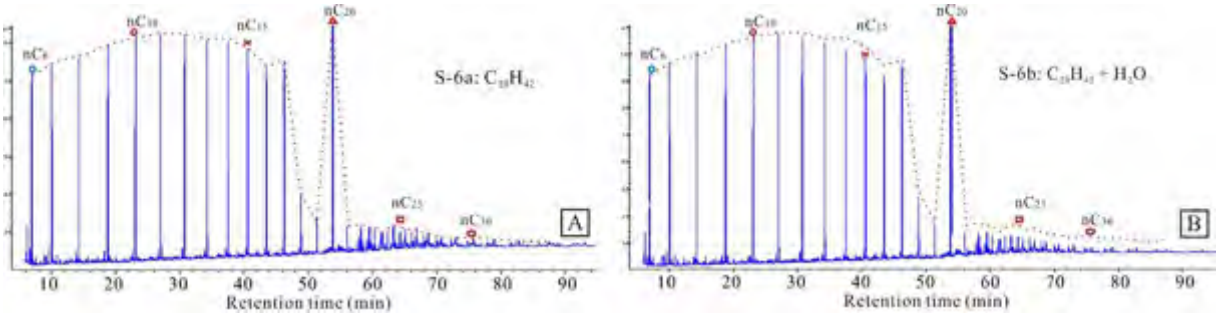

Fig. 10. Gas chromatograms of the samples after the 6-day heating of eicosane in the anhydrous (A) and hydrous (B) systems. The dashed curves represent the pattern of the main compositions of the sample generated in the anhydrous system.

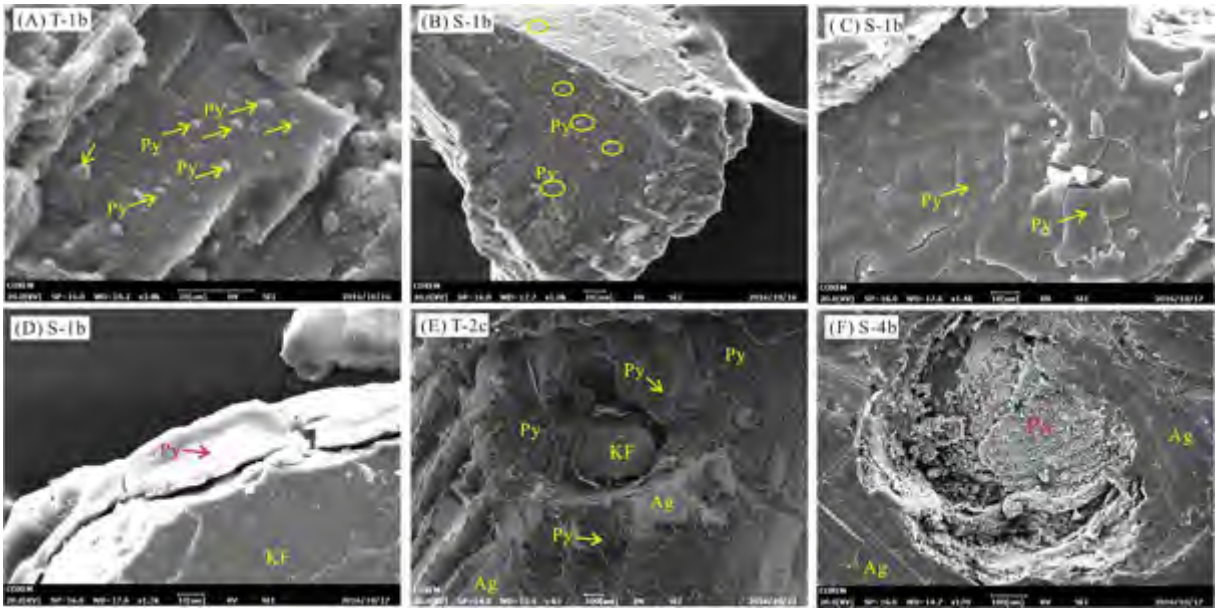

Fig. 11. SEM images of pyrobitumen in different experiments. (A–D) Heavy oil and pyrobitumen (Py) attached to the feldspar surface after reaction in the oil-feldspar system after 2-day (A) or 6-day (B–D) heating; (E) pyrobitumen (Py) coated on the surface of the feldspar grain (KF) and the silver bar (Ag) in the oil zone of the oil-D water- feldspar system (T-2c) after 2-day heating; (F) no pyrobitumen was identified on the surface of the paragonite (Pa) mineral surface and the silver bar in the water zone of the oil-NaCl water-feldspar system (T-4b) after 6-day heating; the enlargement of the paragonite is shown in Fig. 4A.

Table 3
Concentrations of different organic acids in the water after the heating experiments.

Acids	Series												
	2-day						6-day						
	T-2a	T-2b	T-2c	T-4a	T-4b	T-4c	S-2a	S-2b	S-2c	S-4a	S-4b	S-4c	S-6b
Acetic acid	35.38	19.30	21.09	22.78	84.48	67.82	49.40	35.46	40.57	105.43	130.84	60.46	18.30
Oxalic acid	7.71	0.54	5.76	73.47	165.92	72.26	4.82	0.11	0.17	52.90	47.15	54.38	51.82
Methanoic acid	14.55	1.50	1.71	13.64	1.22	5.44	44.32	1.05	2.92	20.56	8.56	4.56	4.48
Propionic acid	8.22	6.13	7.16	53.14	13.24	8.32	9.24	11.84	12.09	14.27	54.08	16.04	6.22

Na^+ and Cl^- in the water results in high concentrations of K^+, Ca^{2+}, and SO_4^{2-} but lower concentrations of Si^{4+} and Al^{3+}. The pH of the water at 30 °C ranges from 5.7 to 6.8.

4. DISCUSSION

4.1. Mineral evolution and acceleration of mineral alteration by oil degradation in oil-water-feldspar system

Minerals (e.g., illite, smectite, calcite, quartz) have been heated in pyrolysis experiments in geochemical systems of oil plus minerals or oil plus water plus minerals in previous studies (Pan et al., 2010; Wang et al., 2015; Xiao et al., 2010). However, the mineral evolution has never been analyzed in these experiments. The detailed SEM and EDS analyses of the mineral phases conducted in this study demonstrate that the mineral evolution in the hot oil-water-rock systems is complex (Figs. 2–5). The mineral reactions that can be identified clearly include feldspar dissolution and precipitation of boehmite, illite and muscovite in the system with D-water, as well as feldspar dissolution and precipitation of boehmite, paragonite and albite in the system with NaCl water.

The minerals and relevant textures identified in the 2-day (T-2b) and 6-day (S-2b) experiments suggest that the mineral alteration reaction pathways in the oil-D water-few feldspar system with a low mineral/fluid ratio and a low Na^+/K^+ ratio are likely to be: feldspar dissolution → boehmite precipitation → boehmite dissolution → illite formation → illite dissolution → muscovite formation (Fig. 3A–C), which is consistent with the reaction pathways at high temperature proposed by Fu et al. (2009) and Zhu et al. (2010). In this system, the feldspar dissolution occurs first and can be represented by reaction-1 (Fig. 3B). With the increase in the concentrations of Al^{3+}, $SiO_{2(aq)}$, and K^+ (Table 4), the precipitation of euhedral boehmite

Table 4
Concentrations of different ions in the water and the tested pH of the water at 30 °C after the heating experiments. The water pH value was tested at room temperature after dissipation of the gases; the actual pH of the 360 °C water after the experiments should be much lower with the presence of CO_2 in the systems. The crude oil is collected from reservoirs with high salinity pore water (Yuan et al., 2015a); the Cl^- and Na^+ in the dehydrated oil should be responsible for the relatively higher concentrations of Cl^- and Na^+ in the D-water system with crude oil than without crude oil.

Ions and pH		Series														
		2-day							6-day							
		T-2a	T-2b	T-2c	T-3	T-4a	T-4b	T-4c	T-5	S-2a	S-2b	S-2c	S-3	s-4a	S-4b	S-4c	S-5
Cations(mg/L)	Al	0.14	0.51	2.52	32.39	0.12	1.37	0.11	0.05	0.22	4.62	1.89	2.521	0.12	0.029	-	0.017
	Si	5.60	125.60	265.00	245.40	6.10	29.94	44.69	35.11	6.46	64.13	293.40	247.80	5.08	39.830	51.33	46.96
	K	3.16	46.80	24.55	16.00	4.44	32.73	830.70	822.30	1.68	34.10	28.62	7.433	4.50	71.530	1544	1022
	Na	31.49	92.87	67.59	57.08	15,840	11,380	14,120	10,040	57.76	64.81	77.21	26.22	15,120	10,800	12,220	11,550
	Ca	1.78	1.79	5.91	1.63	1.53	3.79	9.52	8.91	0.41	0.90	10.48	2.56	2.28	3.57	5.33	6.594
Anion (mg/L)	Cl^-	35.34	147.18	77.76	18.63	15,099	15,989	16,240	15,582	66.25	64.47	95.68	15.11	15,310	15,982	15,368	15,798
	SO_4^{2-}	49.52	3.84	9.22	2.00	59.52	44.82	41.50	69.68	39.65	9.68	19.42	9.81	39.05	70.34	170.92	37.86
pH	30 °C	6.1	6.3	6.4	5.7	5.9	6.0	6.0	6.1	6.3	6.7	6.8	6.0	6.1	6.0	6.0	6.3

(reaction-2) began to occur, which consumed Al^{3+}. With a continued increase in the concentrations of $SiO_{2(aq)}$ and K^+, the precipitation of fibrous illite began to occur (reaction-3), which consumed Al^{3+}, SiO_2, and K^+ (Zhu et al., 2010). The consumption of Al^{3+} resulted in the redissolution of boehmite, which can be verified by the anhedral or small boehmite crystals in the oil-water zone in the 2-day experiment, and by the disappearance of boehmite in the 6-day experiment (Fig. 3A). From boehmite to illite, the whole reaction can be expressed by reaction-4. From the 2-day to the 6-day experiment, the fibrous illite disappeared and plate muscovite was formed. Though illite and muscovite have the same element compositions and similar crystal structures, the processes from illite to muscovite probably involve the dissolution of the fibrous illite and the precipitation of the euhedral muscovite plates. In systems with a high mineral/fluid ratio, after 2-day and 6-day heating, boehmite was not identified but illite and muscovite (Fig. 5A and B) were present (T/S-2c). The lack of the intermediate minerals was probably caused by the rapid increase in ion concentrations (e.g., SiO_2(aq)) (Table 4) in the systems, with existence of higher mineral reactive surface areas in such systems (Helgeson, 1979; Yuan et al., 2017; Zhu et al., 2010). The reactions in systems with such a high mineral/fluid ratio probably include reaction-1 and reaction-3 and the overall reaction can be expressed by reaction-5. All chemical reactions (1–5) involve the participation of H^+ (Fig. 3B) and the H^+ consumed by the mineral alterations may be provided by CO_2 and organic acids (Figs. 6A, B and 8C). Additionally, OH^- is present in all secondary minerals including boehmite, illite, and muscovite (Fig. 3C) (Hu et al., 2003; Raybaud et al., 2001).

The mineral alteration reaction pathways in the oil-NaCl water-few feldspar system with a low mineral/fluid ratio and a high Na^+/K^+ ratio (T/S-4b) are likely to be: K-feldspar dissolution → boehmite precipitation → boehmite dissolution → paragonite formation → paragonite dissolution → albite formation (Fig. 4A) (Helgeson, 1979; Lu et al., 2013). The relevant chemical reactions can be described by reactions 6–12 (Fig. 4B). The mineral textures (Fig. 4) in systems T/S-4b support the precipitation and redissolution of boehmite and paragonite in the 2-day and 6-day experiments. Different from the system with D-water, the final-step mineral is not phyllosilicate paragonite (Fig. 3C) but framework albite (Fig. 4C). The albite can be formed by reaction-12 through the dissolution of paragonite and then the precipitation of albite or by reaction-13 through direct replacement of the K-feldspar. In systems with a high mineral/fluid ratio, after 2-day and 6-day heating, boehmite was not identified but paragonite and albite (Fig. 5D–F) were identified in the oil-NaCl water-feldspar system (T/S-4c), which was likely caused by the rapid increase in ion concentrations (e.g., $SiO_{2(aq)}$) (Table 4) in the systems due to the presence of higher mineral reactive surface areas in such systems.

The big difference between the Na^+/K^+ ratios (Table 4) should be responsible for the formation of the K-rich minerals (illite, muscovite) and Na-rich minerals (paragonite, albite) in the two different types of systems (Bjørkum and Gjelsvik, 1988; Bjørlykke and AAgaard, 1992; Fu et al.,

2009). In the T/S-2b system with a low Na^+/K^+ ratio, K^+ have the capacity to compete with Na^+ to combine with Si^{4+} and Al^{3+} to form illite and muscovite, which is verified by the EDS composition data of the fibrous and plate minerals (Fig. 3). In contrast, in the T/S-4b system with a very high Na^+/K^+ ratio, K^+ cannot compete with the high concentration of Na^+. Si^{4+} and Al^{3+} combine with Na^+ to form paragonite and albite, which is also verified by the EDS data of the minerals (Fig. 4). The formation of such Na-rich minerals also results in lower concentrations of Si and Al (Table 4).

The development of different minerals indicates the existence of different ion concentrations in the water, water-oil, and oil zones (Bjørlykke and AAgaard, 1992; Yuan et al., 2017), which still cannot be studied using the available average concentrations of the various solutes. It is difficult to determine the quantitative saturation of oil and water in the three different zones; however, the identified mineral evolutions in these zones indicate that the chemical diagenesis in the reservoirs does not cease if some pore water is still present in the rocks after oil charging (Figs. 3 and 4). The abovementioned mineral evolution pathways and the mineral differences in the water, oil-water, and oil zones in a specific system even demonstrate that the mineral alteration progresses faster in the oil zone than in the water zone (Figs. 3 and 4), indicating that the oil degradation may accelerate the mineral alterations.

4.2. Oil degradation in anhydrous and hydrous systems

The GC chromatograms of the liquid oil samples (Fig. 9) and the various gases (Fig. 6A and B) after the experiments show that the degradation of high-molecular hydrocarbons (C_{17}–C_{33}) dominates the processes in the 2-day experiments. As the experiments continue, more high-molecular hydrocarbons were degraded and an additional degradation of some middle-molecular hydrocarbons (C_{12}–C_{16}) occurred (Fig. 9). The relative lighter $\delta^{13}C$ compositions of the generated methane to propane (C_1–C_5 *n*-alkanes including *iso*-alkanes) in the 6-day experiments compared to the 2-day experiments (Fig. 6C) also verified that the degradation of some relative low-molecular hydrocarbons (C_{12}–C_{16}) occurred in the 6-day experiments (Fig. 9) (Guo et al., 2009; Tian et al., 2010).

4.2.1. Reaction pathways of oil degradation in the anhydrous system

It has been verified by many previous studies that the anhydrous oil degradation proceeds mainly through the free radical mechanism (Hill et al., 2003; Lewan, 1997; Tian et al., 2006). The extremely low amounts of *i*-C_4 and *i*-C_5 (Fig. 7A and C) and the wide distribution of the low-molecular-weight *n*-alkanes (C_1–C_{19}) (Fig. 10) in the eicosane-containing system after the 6-day heating support the occurrence of the free radical thermal cracking reaction; the presence of the high-molecular-weight organics (C_{21}–C_{33}) and the H_2 demonstrates the occurrence of the free radical cross-linking reaction in the eicosane degradation processes at the temperature of 360 °C. In addition, the absence of CO_2 in the gases rules out of oxidation of the free radicals in the anhydrous eicosane system (Fig. 7, Table 2).

The ratios of *i*-C_4/*n*-C_4 and *i*-C_5/*n*-C_5 in the oil-containing system (Fig. 8A) in this study are similar to the data in the anhydrous oil pyrolysis experiments conducted by Pan et al. (2010). The low concentrations of the branched alkanes (Figs. 6A, B and 8A) and the wide distribution of the low-molecular-weight *n*-alkanes (C_1–C_{15}) (Fig. 9) suggest that the free-radical mechanism probably dominated the oil degradation reactions in the anhydrous hydrous systems in the present study (Hill et al., 2003; Lewan, 1997). The generation of *i*-C_4 and *i*-C_5 in the oil-containing systems are likely to be produced mainly by the degradation of Pr, Ph, and some other high-molecular iso-alkanes (Fig. 9). The low yield of the C_1–C_5 gases, the very low yields of CO_2, the high generation of H_2 (Fig. 6), and the wide distribution of pyrobitumen (Fig. 11A–D) in the anhydrous T/S-1a and T/S-1b systems suggest that the free radical cross-linking and the free radical thermal cracking are both important in the anhydrous oil degradation processes (Hill et al., 2003; Lewan, 1997).

4.2.2. Promoting effect of water on oil degradation

The experimental data show that after 6-day heating, the yields of C_1–C_5 and CO_2 in the hydrous eicosane-containing system are much higher than those in the anhydrous system (Fig. 7A). Similarly, the experimental data show that after heating for two days and six days, much larger amounts of hydrocarbon gases (C_1–C_5), low molecular liquid C_6–C_7, and CO_2 were yielded in the hydrous oil-containing experiments than in the anhydrous oil-containing experiments (Figs. 6 and 9). In addition, various organic acids were generated during the oil (eicosane) degradation processes in the hydrous systems (Figs. 7D and 8C). High pressure has been verified to suppress oil degradation (Chen et al., 2014; Hill et al., 1996; Uguna et al., 2016). Though pressure was not monitored in the present study, the hydrous systems with less vacant space and more gases in the gas zones (Fig. 1) suggest that the pressure should be higher in the hydrous systems than in the anhydrous systems. Thus, the high yield of the low-molecular hydrocarbons (Figs. 6 and 7) and the low abundance of the remnant high-molecular hydrocarbons (Fig. 9) in the hydrous system suggest that water promoted the oil (eicosane) degradation reactions in the present study. This result is in agreement with some previous studies (Shuai et al., 2012; Wang et al., 2015), although some other researchers claimed that water retards oil degradation (Hesp and Rigby, 1973; Lewan, 1997; Price, 1993; Uguna et al., 2016) or has little impact on oil degradation (Xie et al., 2016). The oil-NaCl water systems generate even more gases, liquid hydrocarbons, and organic acids than the oil-D water systems (Figs. 6, 8 and 9), which may be due to the presence of Cl^- anions, which are good nucleophiles that favor the hydrocarbon decomposition by attacking the C—C bond (e.g., methyl group) at elevated temperatures (Bu et al., 2017; Cui et al., 2008).

4.2.3. Influence of water on isomerization

The ratios of *i*-C_4/*n*-C_4 and *i*-C_5/*n*-C_5 are generally slightly higher in the hydrous oil (eicosane) plus D-water systems (with or without feldspar grains) than in the anhydrous system (Figs. 7C and 8A), indicating that the isomerization in the hydrous system was not promoted extensively via the carbocation mechanism (Bu et al., 2017; Lewan, 1997; Seewald, 2003), which is associated with the Brønsted (B) acid sites in the secondary minerals including boehmite, illite and muscovite (Liu, 2001; Liu et al., 2014, 2013). In the hydrous system with NaCl water, the ratios of *i*-C_4/*n*-C_4 and *i*-C_5/*n*-C_5 exhibit little difference to the ratios of the anhydrous system (Fig. 8A), suggesting that the oil degradation via carbocation mechanism did not occur and indicating that the B acid sites in the secondary minerals including boehmite and paragonite may have been suppressed by the high concentrations of Na^+ or Cl^-. Although water molecules associated with a high concentration of Na^+ have been suggested to act as Brønsted acid sites because they are strongly dissociated and capable of providing protons (Bu et al., 2017), it does not appear that this mechanism occurred in the present experiments. Therefore, the free-radical mechanism probably also dominated the oil degradation reactions in the hydrous systems in this study, which is also verified by the low concentration of the branched alkanes (Figs. 6 and 7) and the wide distribution of the low-molecular-weight *n*-alkanes (C_1–C_{15}) (Figs. 9 and 10) (Lewan, 1997; Seewald, 2003). Similar to the anhydrous systems, most *iso*-butane and *iso*-pentane may be produced by the degradation of Pr and Ph (Fig. 9).

4.2.4. Influence of water on the ratios of different gases and pyrobitumen

In this study, the C_2H_4/C_2H_6 and C_3H_6/C_3H_8 ratios are much lower in the hydrous experiments than the anhydrous experiments (Figs. 7C and 8B) and the pyrobitumen in the hydrous system can only be identified in the upper oil zone (Fig. 11E and F). The low yield of ethylene and propene probably occurred because the produced gas olefins are unstable and are readily transformed to saturated hydrocarbons during the thermal experiments in the hydrous system (Bu et al., 2017). The presence of water probably results in the high yield of H_2 in the 2-day hydrous experiments (Fig. 6A). From the 2-day to the 6-day experiments, much more H_2 was generated in the anhydrous system during the cross-linking reaction processes (Fig. 6B) and the H_2 was not consumed by the olefins, including ethane and propylene. In the hydrous experiments, however, not much additional H_2 was generated after the 6-day heating (Fig. 6B). The extra hydrogen from the water should have been consumed to form the high yield of the low-molecular alkanes (Figs. 6B and 8A), indicating that the presence of water can promote thermal cracking to form more low-molecular alkanes but not alkanes (Lewan, 1997). With hydrogen serving as an intermediate species, the small difference between the H_2 yield in the 2-day and 6-day hydrous experiments (Fig. 6A and B) suggests the existence of a possible metastable equilibrium in the gas-oil-water system (Helgeson et al., 1993).

The presence of water decreases the ratios of C_1/C_2, C_2/C_3, C_1/C_2+C_3 and C_1/C_1-C_5 (Fig. 8A) in the oil-containing system, whereas the presence of water in the eicosane-containing system increases the ratios of C_1/C_2, C_1/C_2+C_3 and C_1/C_1-C_5. These variations may have occurred because free-radical sites tend to develop at different carbon positions of different long-chained hydrocarbons in the anhydrous and hydrous system, and this may lead to thermal cracking of long-chained hydrocarbons to form lower-molecular alkanes with different carbon number.

4.2.5. Influence of water on isotopic fractionation

The $\delta^{13}C$ data of the alkanes are 1–2‰ lighter in the hydrous experiments than in the anhydrous experiments (Figs. 6C, 7B and Table 2). Because the 6-day experiments that have experienced extensive oil decomposition also have lower $\delta^{13}C$ data (2–3‰) than the 2-day experiments, the isotopic difference between the hydrous and anhydrous systems may have been caused by the extensive oil decomposition, particularly the degradation of moderate molecular alkanes in the hydrous system (Fig. 9).

The $\delta^{13}C$ data of CO_2 are 2–5‰ lighter in the hydrous than in the anhydrous system and the difference is particularly significant in the 6-day experiments (Fig. 6C). The extensive oil decomposition in the hydrous system (Fig. 9) may have contributed to this isotopic difference. However, the isotopic difference between the 6-day and 2-day experiments under the same conditions is generally less than 1–3‰, indicating that the difference in oil degradation between the hydrous and anhydrous systems alone cannot explain the big isotopic differences. Some other reactions (e.g. decarboxylation, oxidation of organic materials, dissolving in and out of water) may have affected the isotopic fractions of ^{13}C among the CO_2 and relevant precursors, although the detailed reason is still unclear.

4.2.6. Reaction pathways of oil degradation in the hydrous system

The presence of water in the hydrous system can provide different pathways for the decomposition of the transition-state molecules formed by the free-radical mechanism, with an additional supply of hydrogen and hydroxyl (Seewald, 2001, 2003). The high yield of the low-molecular alkanes, the low ratio of alkenes/alkanes, the lower generation of pyrobitumen, the high-molecular hydrocarbons and H_2, and the presence of large amounts of organic acids and CO_2 in the hydrous oil- and eicosane-containing experiments (Figs. 6–11) suggest that the oil degradation in the presence of water proceeded at least in four different pathways (Fig. 12): (1) free-radical cross-linking of the C—C bonds to form pyrobitumen and H_2 (Hill et al., 2003); (2) free-radical thermal cracking of C—C bonds to form low-molecular alkanes with the absorption of hydrogen originating from water and the cross-linking reactions (Hill et al., 2003); (3) oxidation of free radicals to form alcohols and the successive oxidative decomposition of alcohols to form organic acids with the absorption of hydroxyl originating from water (Seewald, 2001, 2003); and (4) decarboxylation of organic acids to form CO_2 and short-chain saturated hydrocarbons (Bu et al., 2017; Seewald, 2001,

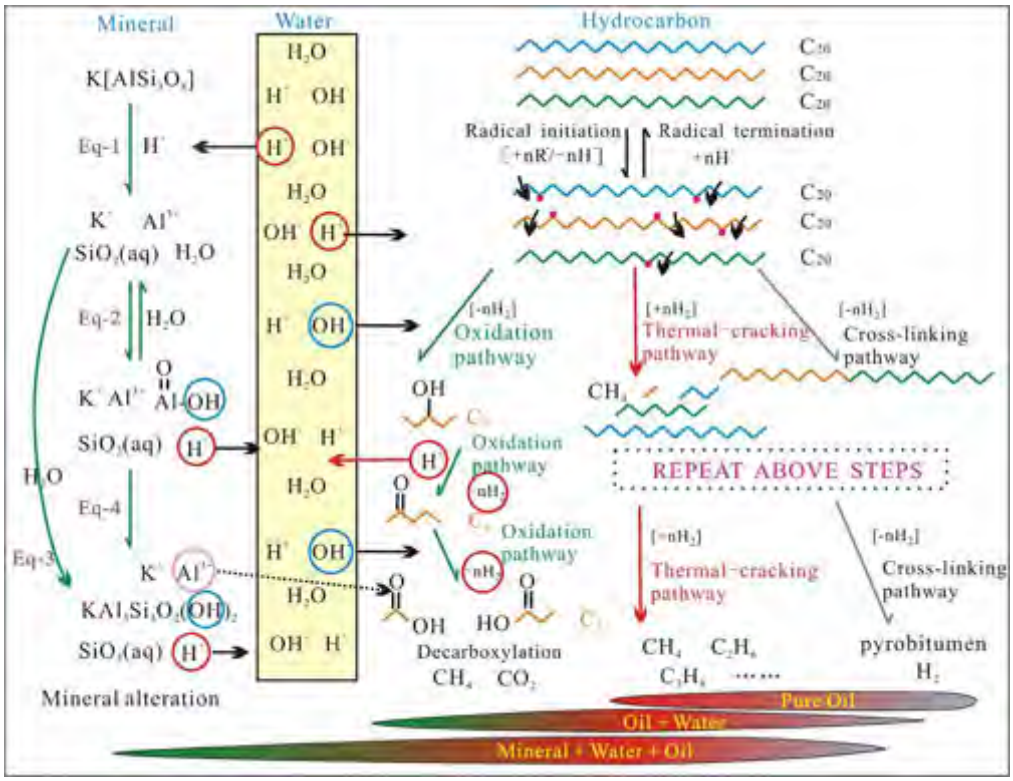

Fig. 12. Various reaction pathways for hydrocarbon degradations in different geochemical systems.

2003). With the participation of water and an extra supply of hydrogen, pyrobitumen exists commonly only in the oil zone in the oil-water-feldspar system (silver bar in Figs. 1A and 11E, F), indicating that thermal cracking probably exceeds cross-linking to generate more low-molecular alkanes and less pyrobitumen in the hydrous system.

4.3. Impact of mineral alteration on oil degradation

4.3.1. Promoting/inhibiting effect of mineral alteration on oil degradation

The experimental data from the oil-D water-(feldspar) systems (T/S-2a, b, c) show that the presence of large amount of minerals (or mineral reactions) promotes the oil degradation to generate more C_1–C_5 alkanes (Fig. 6A and B), C_{10}–C_{15} alkanes (Fig. 9D–F), CO_2 (Fig. 6A and B), and organic acids (Fig. 8C); however, the generation of H_2, C_6–C_9 *n*-alkanes, cyclopentane, methyl-cyclohexane, toluene, and xylene is significantly inhibited (Figs. 6A, D, 9D–F and Table 2). The less generation of H_2 should have been caused because hydrogen was consumed to generate more C_1–C_5 alkanes (Bu et al., 2017; Lewan, 1997). Different from the oil-D water-(feldspar) system, data from the oil-NaCl water-(feldspar) systems (T/S-4, a, b, c) demonstrate that the mineral alteration reactions in systems with high Cl^- concentrations suppressed the oil degradation processes, resulting in less generation of H_2, CO_2, organic acids, low-molecule alkanes (C_1–C_{10}), cyclopentane, methyl-cyclohexane, toluene, and xylene (Figs. 6A, B and 9G–I). These large differences between the oil-D water-feldspar and the oil-NaCl water-feldspar systems suggest that the mineral reactions in different hydrogeochemical systems result in different impacts on the oil degradation processes.

4.3.2. Influence of mineral alteration on isomerization

The test data show that the ratios of *i*-C_4/*n*-C_4 and *i*-C_5/*n*-C_5 are almost identical in the hydrous D-water (NaCl) systems with or without feldspars (Fig. 8A), indicating that the oil degradation via the carbocation mechanism is relatively limited in the systems with minerals including feldspar, boehmite, illite, and paragonite. The B acid sites in these minerals (Figs. 3C and 4C) probably have limited impact on oil degradation. The low concentration of branched alkanes (Fig. 6A and B) and the wide distribution of low molecular-weight *n*-alkanes (C_1–C_{15}) (Fig. 9) suggest that the free-radical mechanism probably also dominates the oil degradation reactions in the systems with extensive mineral reactions (Lewan, 1997; Seewald, 2003), in which most of the *iso*-butane and *iso*-pentane are also generated by the degradation of Pr and Ph (Fig. 9).

4.3.3. Influence of mineral alteration on ratios of different gases

For the systems with oil plus water, the addition of large amounts of feldspar minerals generally further decreases the ratios of C_2H_4/C_2H_6 and C_3H_6/C_3H_8 (Fig. 8B). In

addition, the amount of produced H_2 decreased (Fig. 6A and B). As mineral degradation promotes oil degradation overall, the decrease of H_2 in the system with large amounts of feldspars indicates that H_2 should have been consumed to form the high yield of the low-molecular alkanes (Fig. 6A and B), indicating that the presence of extensive mineral reactions (or the H^+ participating in the reactions) promoted thermal cracking to form more low-molecular alkanes but not alkanes.

Aside from the alkene/alkane ratios, the presence of large amounts of feldspars also decreases the ratio of C_1/C_2, C_2/C_3, $C_1/C_2 + C_3$, and C_1/C_1–C_5 (Fig. 8A) in the system with D-water. These results have two implications: first, the C_2 and C_3 are more stable in the D-water hydrous environments with mineral reactions; second, free-radical sites tend to develop at different carbon positions of the long-chained hydrocarbons in the hydrous system with extensive mineral alteration. Contrary to the D-water system, the addition of 1 g of feldspar to the NaCl system increased the ratios of C_1/C_2, C_2/C_3, $C_1/C_2 + C_3$, and C_1/C_1–C_5, suggesting that C_1 is more stable in the oil NaCl-water hydrous systems with mineral reactions. These differences between the oil-D water-feldspar and the oil-NaCl water-feldspar systems also suggest that the mineral reactions in different hydrogeochemical systems result in different impacts on the oil degradation processes.

4.3.4. *Influence of mineral alteration on isotopic fractionation*

The isotope differences in the specific gases for the systems with and without feldspars are generally very small (<1‰) (Fig. 6C) and this may have been caused by the difference in the degree of oil decomposition between the systems (Fig. 9), indicating that the mineral reactions are likely to have little impact on the isotopic fractionation during oil degradation processes.

4.4. Bridging function of water and pathways of oil-water-mineral interactions

Very few small pits on some feldspar grains (Fig. 2B and C) occur in the anhydrous oil-feldspar systems after 2–6 days of heating and secondary minerals were not identified. In turn, the addition of feldspars to the oil also has little effect on the yield of the various gases in the anhydrous system (Figs. 6A, B and 9B, C). These results demonstrate that a direct geochemical interaction between the feldspar and the oil is extremely limited without the presence of water as a matrix, solvent, and reactant for the hydrogeochemical reactions (Schulz et al., 2015).

On the one hand, water promotes the oil degradation reactions (Figs. 6 and 9) (Shuai et al., 2012; Wang et al., 2015). On the other hand, water dissolves feldspar minerals and forms new minerals (Fig. 2) (Glasmann, 1992; Yuan et al., 2015b; Zhu et al., 2010). As aforementioned, in the presence of water in the oil-water-feldspar system, feldspar is leached extensively to form secondary minerals and the mineral transformations are accelerated by the oil degradation (Figs. 3 and 4). At the same time, the oil degradation is promoted (or suppressed) by the mineral alteration in the oil-D water (or NaCl water)-feldspar systems (Figs. 6 and 9). The extensive mineral alteration and yield variations of the low-molecular-weight hydrocarbons in the oil-water-feldspar systems suggest that water serves as a critical bridge between the organic and inorganic reactions (Cai et al., 2012; Seewald, 2003).

The mineral transformation from the initial K-feldspar to boehmite, illite, and muscovite in the oil-D water- feldspar system are controlled by changes in the concentrations of the dissolved Al^{3+}, SiO_2, K^+, and the pH of the aqueous phase (Bjørkum and Gjelsvik, 1988; Fu et al., 2009; Helgeson, 1979; Zhu et al., 2010). All reactions at each step involve the participation of H^+ and OH^- (Figs. 3B–C and 4B–C) (Zhu et al., 2010). Similar to the water-mineral reactions, the hydrous oil (eicosane) degradation processes including the cross-linking, thermal cracking, and oxidization reactions also involve the participation of H^+ and OH^- (Fig. 12) (Lewan, 1997; Seewald, 2001, 2003). Organic acids and CO_2 can also be ionized in water to produce H^+ (Giles, 1986; Surdam and Crossey, 1987; van Berk et al., 2013; Yuan et al., 2017).

At elevated temperatures, water acts as a solvent of ions (Al^{3+}, SiO_2, K^+, Na^+) required for mineral alterations, H^+, OH^-, CO_2, low-molecular organic acids, and some hydrocarbons (Lewan, 1997; Seewald, 2003; Surdam and Crossey, 1987; Yuan et al., 2017; Zhu et al., 2010). The H^+ and OH^- ions from different origins are dissolved in water and probably serve as the bridge linking the mineral alteration reactions and the oil degradation reactions with exchanges of these ions occurring among minerals, water, and organic matter (Fig. 12). As aforementioned, the Brønsted acid sites in the secondary minerals including boehmite, illite, and muscovite have a relatively limited ability to promote oil degradations in our experiments. Thus, these ion mutual exchanges are the most likely mechanism resulting in the mutual promotion of overall oil degradation and mineral alteration in the oil- D water-feldspar system.

Additionally, the Lewis acid sites in the feldspar, illite, and muscovite (Figs. 3C and 4C) may promote the decarboxylation of organic acids to form more low-molecular alkanes and CO_2 (Bu et al., 2017). However, after the consumption due to the interactions with the minerals, the remaining CO_2 and organic acids in systems with large amounts of minerals do not have a high yield (Figs. 6 and 8C). Overall, the extra supply of hydrogen and hydroxyl ions originating from water and minerals promotes the thermal cracking and suppresses the cross-linking (Lewan, 1997; Seewald, 2001). However, an understanding of the mechanisms of the suppression of the generation of C_6–C_9 aliphatics still requires further studies.

In the oil-NaCl water-feldspar system (T/S-4c), the suppression of the oil degradation by the mineral reactions (compared with T/S-4a, b) may be caused by two reasons. First, the Brønsted acid sites in the secondary minerals (e.g., boehmite, paragonite) (Brown and Nadeau, 1984; Deer et al., 2013; Raybaud et al., 2001) may compete with the halide anion (Cl^-), leading to a low generation of low-molecular alkanes (Bu et al., 2017). Second, K-feldspar was replaced by albite (Fig. 4) with a direct substitute of K^+ by Na^+ in the system with high ratios of rock/water and

Na^+/K^+ (Helgeson, 1979; Lu et al., 2013; Yuan et al., 2017; Zhu et al., 2010). Without the formation of intermediate boehmite and paragonite, little interchange of H^+ or OH^- occurred between the minerals and hydrocarbons.

4.5. Geological implications

The present experiments demonstrate that the organic-inorganic interactions in oil-water-rock systems at elevated temperatures are complex. Smectite and mixed layer illite-smectite (I/S) clays have been proved to affect the oil generation and degradation in anhydrous pyrolysis systems without the presence of external water (Bu et al., 2017; Cai et al., 2012; Li et al., 2016; Pan et al., 2010). Unlike these minerals that contain interlayer water, the organic-inorganic interactions between oil and minerals without interlayer water (e.g., feldspar) are likely to be linked and promoted by ambient water. Additionally, the type of water also has a great impact on the coupled organic-inorganic interactions and affects the stabilities of aqueous hydrocarbons as well.

Different from shale rocks that contain large amounts of smectite and I/S clays (Berger et al., 1997; Li et al., 2016; Lynch et al., 1996; Macquaker et al., 2014; Milliken, 1992), deeply buried arkose sandstone reservoirs generally contain silicate minerals without interlayer water (e.g., large amounts of feldspar, few percent of illite) (Glasmann, 1992; Yuan et al., 2015a, 2015b, 2017). In such reservoirs, the water and oil saturations in the reservoirs probably affect the occurrence and evolution of the organic-inorganic interactions (van Berk et al., 2013; Worden et al., 2017). The organic-inorganic interactions in different oil, oil-water, and water geochemical systems in a reservoir proceed in different reaction pathways and may lead to different impacts on deeply-buried hydrocarbon arkose reservoirs (Fig. 13). In accordance to previous concepts (Hill et al., 2003; Tian et al., 2010) and the presented anhydrous experiments under elevated temperatures, we propose that the oil degradation in the oil leg of a reservoir proceeds mainly through the free radical cross-linking reaction and the free radical thermal cracking reaction, resulting in the generation of liquid and gaseous hydrocarbons, large amounts of insoluble bitumen (e.g., pyrobitumen), and H_2 but small amounts of CO_2 and organic acids. The overall hydrocarbon quality is degraded due to the generation of large amounts of pyrobitumen. At the same time, the reservoir quality is reduced because the pyrobitumen occupies pores and pore-throats in the rocks. The oil degradation at the oil-water transition zone (OWTZ) of an arkose reservoir proceeds via at least the above-mentioned four pathways (Fig. 12) (Lewan, 1997; Seewald, 2001, 2003; van Berk et al., 2013). The extra supply of hydrogen and hydroxyl ions provided by the water promotes the thermal cracking reaction pathway and suppresses the cross-linking pathway; the oil degradation generates large amounts of liquid and gaseous hydrocarbons, organic acids, and CO_2 but little hydrocarbon in the OWTZ. Many secondary pores can be generated because the organic acids and CO_2 promote leaching of the silicate minerals (e.g., feldspar) in the rocks (Yuan et al., 2018) and these secondary pores can serve as spaces for newly charged hydrocarbons. Because the silicate mineral alteration reactions retard the overall oil degradation reactions in systems where saline pore water is present, the liquid hydrocarbons in the OWTZ of a reservoir may be preserved in deep layers over geological time. Thus, the organic-inorganic interactions are likely to improve the quality of both the hydrocarbon and the reservoir in the OWTZ. Because the stabilities of aqueous hydrocar-

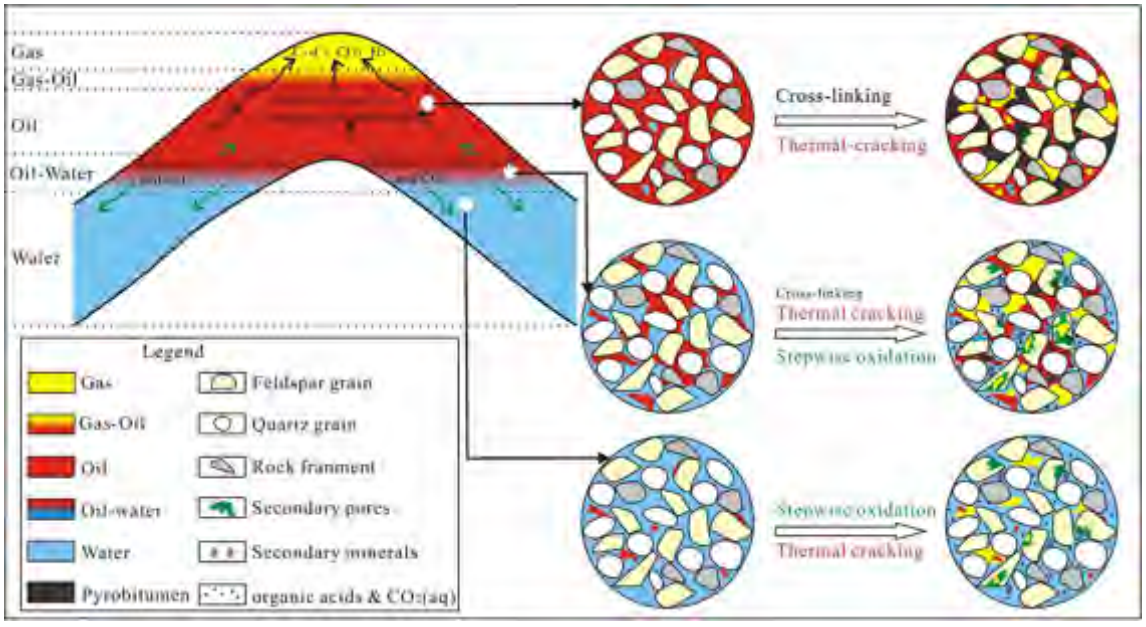

Fig. 13. Schematic diagram showing the evolution of the organic-inorganic interactions in different zones in an arkose reservoir.

bons and the reaction pathways of the mineral alteration and oil decomposition are strongly influenced by the organic-inorganic interactions, the incorporation of such complex organic-inorganic interactions into geochemical models will improve the quantitative prediction of hydrocarbons and reservoir spaces in natural environments over geologic time (Lewan, 1997; Seewald, 2001, 2003).

The experiments in this study were conducted at a high temperature (360 °C) beyond the temperature of natural hydrocarbon reservoirs for the purpose of accelerating the oil degradation reactions. The high temperature may have changed the mineral reactions pathways (e.g., feldspar-gibb site-kaolinite-illite in D-water system) at low temperatures (80–200 °C) to the present pathways (e.g., feldspar-boeh mite-illite-muscovite in D-water system) at high temperatures (Bjørkum and Gjelsvik, 1988; Fu et al., 2009; Helgeson, 1979; Lu et al., 2013; Pan et al., 2010). The essence of such reactions are similar because the series of minerals contain similar crystal structures and the intermediary H^+ agent is involved in both these two series of reactions (Zhu et al., 2010). Thus, the results of these experiments are likely to be applicable at a relative low temperature range. For example, the deeply-buried Eocene reservoirs in the Minfeng subsag (4100–4400 m) of the Dongying Sag, as well as in the Bonan subsag (4000–4300 m) of the Zanhua Sag are both characterized by extensive oil decomposition and high pore-water salinity (extremely high Cl^- and Na^+ concentrations) (Li et al., 2010; Ping et al., 2010; Song et al., 2009). Feldspar dissolution is extensive and albite, illite and quartz overgrowths have been identified as important secondary minerals in these reservoirs (Ma et al., 2017; Tian et al., 2015; Wang et al., 2016). The pyrobitumen in these reservoirs and the chemistry of natural gas demonstrate that oil degradation contributes significantly to the natural gases in these reservoirs (Li et al., 2010; Ping et al., 2010). The current temperature (155–165 °C) of these Eocene reservoirs, a critical temperature for the occurrence of extensive oil degradation (Waples, 2000), is the highest temperature these reservoirs have experienced (Song et al., 2009). The extensive decomposition of crude oil in these reservoirs is likely due to the high pore-water salinity, which is in accordance with the results of this study. With regard to the problems associated with low temperatures and geologic time scale in natural reservoirs, we are conducting on-going experiments at 180 °C designed to run ½–1 year and expected to provide more practical results with direct geological implications.

5. CONCLUSIONS

(1) The experimental results of this study clearly demonstrate that organic-inorganic interactions do occur in oil-water-mineral systems at elevated temperatures. The extensive interactions between organic oil and inorganic feldspar were induced by water. The mutual exchanges of H^+ and OH^- between oil, water, and minerals are the most likely mechanisms resulting in the mutual impact of oil degradation and mineral alteration.

(2) The organic-inorganic interactions are complex in oil-water-rock systems. Water (particularly water with a high concentration of Cl^-) promotes the oil degradation significantly. The presence of water introduces more degradation pathways for oil degradation, leading to the generation of more CO_2 and organic acids. The water chemistry affects the mineral evolution greatly. In the oil-water-feldspar system, a low Na^+/K^+ ratio results in the formation of secondary minerals with more potassium (illite and muscovite), whereas a high Na^+/K^+ ratio results in the formation of secondary minerals with more sodium (paragonite, albite).

(3) The mineral alteration does not occur in the presence of pure oil. In the oil-water-rock system, the mineral alternations do not stop, even in the oil zone in the presence of some water and the oil degradation can even accelerate the mineral alteration reactions. In turn, the mineral reactions in different water systems have different impacts on oil degradation. Aluminosilicate mineral alterations promote the oil degradation in a geochemical system with D water but retard the oil degradation in a geochemical system in high salinity NaCl-water.

(4) Hydrocarbons, water, and minerals are closely associated in deeply-buried sedimentary basins; therefore, the organic-inorganic interactions are an unavoidable consequence during sediment alteration processes. Thus, it is essential to consider the role of water and minerals in experimental studies designed to quantitatively determine the oil degradation and understand the role of oil degradation in mineral alterations. In addition, models aimed at accurate prediction of the evolution of organic and inorganic species in petroleum reservoirs should integrate both organic and inorganic geochemical processes and the relevant kinetics.

ACKNOWLEDGMENTS

This study was funded by the Natural Science Foundation of China Project (No. 41602138; U1762217; 41872140), the National Science and Technology Special Grant (No. 2016ZX05006-007; No. 2016ZX05006-003), and the Fundamental Research Funds for the Central Universities (15CX08001A, 18CX07007A). Prof. Liu Jinzhong, Prof. Tian Hui, Dr. Chen Jian, Li Yong at the State Key Laboratory of Organic Geochemistry of the Guangzhou Institute of Geochemistry, Yu Ying at the Analytical and Measurement Research Center of the Qingdao Institute of Oceanology are thanked for their assistance in the experiments and sample tests. We sincerely thank GCA associate editor Dr. Thomas Wagner and another two anonymous reviewers for reviewing our work and for their great advices and constructive comments.

APPENDIX A

See Fig. A1 and Table A1.

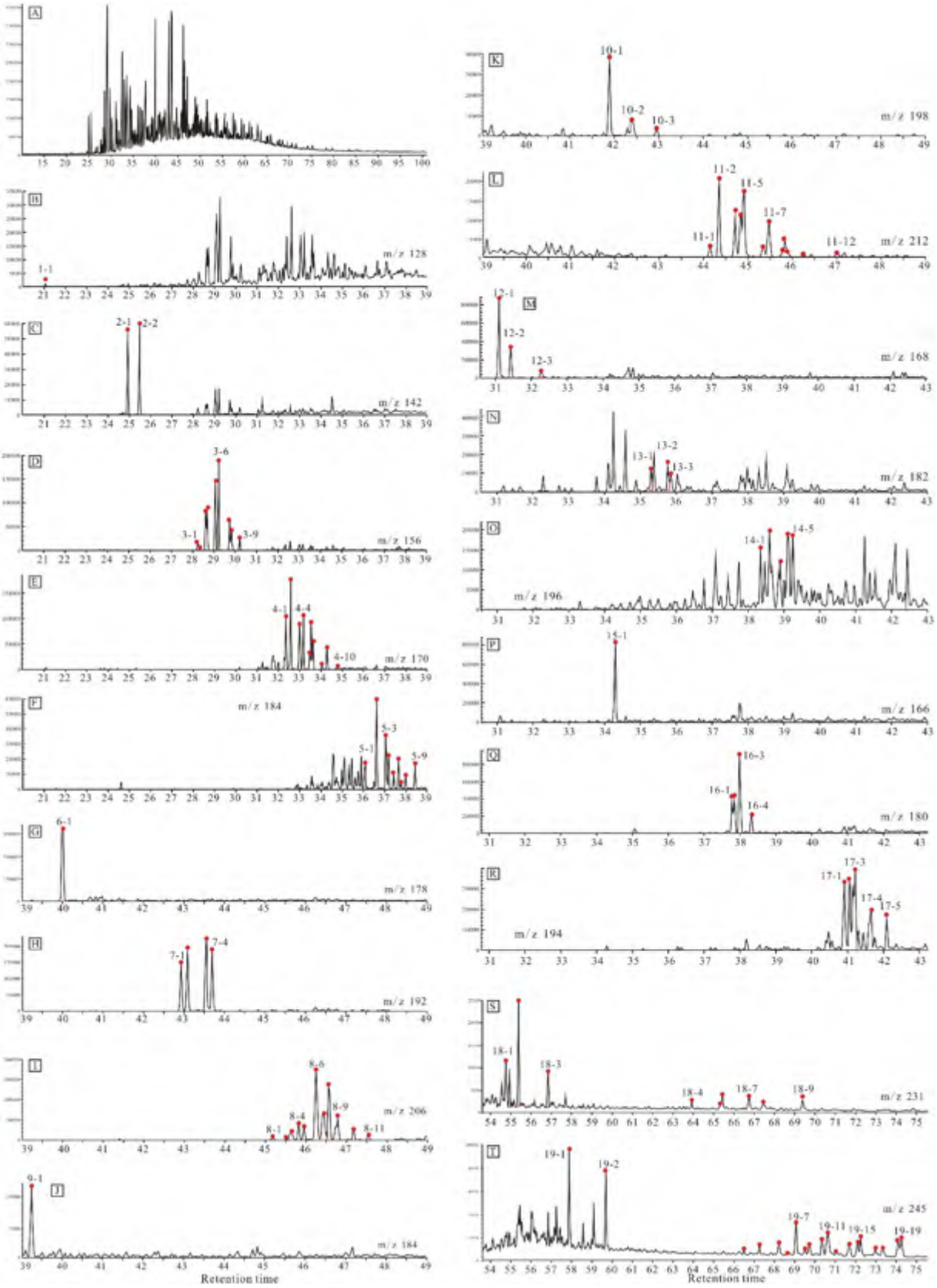
A
B
m/z 128
1-1
C
2-1
2-2
m/z 142
D
3-6
3-1
3-9
m/z 156
E
4-1
4-4
4-10
m/z 170
F
m/z 184
5-3
5-1
5-9
G
6-1
m/z 178
H
7-1
7-4
m/z 192
I
8-6
8-4
8-9
8-1
8-11
m/z 206
J
9-1
m/z 184
Retention time
K
10-1
10-2
10-3
m/z 198
L
11-2
11-5
11-7
11-1
11-12
m/z 212
M
12-1
12-2
12-3
m/z 168
N
13-2
13-1
13-3
m/z 182
O
14-1
14-5
m/z 196
P
15-1
m/z 166
Q
16-3
16-1
16-4
m/z 180
R
17-3
17-1
17-4
17-5
m/z 194
S
18-1
18-3
18-4
18-7
18-9
m/z 231
T
19-1
19-2
19-7
19-11
19-15
19-19
m/z 245
Retention time

Table A1
Types and content of various compositions in the aromatics. Label No. is available in Fig. A1.

Label No.	Retention time	Compound name	Formular	Peak area	Content in the aromatics (%)
1–1	21.048	Naphthalene	$C_{10}H_8$	53,242	0.04
2–1	24.967	2-Methyl naphthalene	$C_{11}H_{10}$	1,664,202	1.17
2–2	25.522	1-Methyl naphthalene	$C_{11}H_{10}$	1,658,216	1.16
3–1	28.26	2-Ethyl naphthalene	$C_{12}H_{12}$	380,652	0.27
3–2	28.32	1-Ethyl naphthalene	$C_{12}H_{12}$	115,055	0.08
3–3	28.641	2,6-Dimethyl naphthalene	$C_{12}H_{12}$	1,560,530	1.10
3–4	28.704	2,7-Dimethyl naphthalene	$C_{12}H_{12}$	2,768,317	1.94
3–5	29.094	1,3 + 1,7-Dimethyl naphthalene	$C_{12}H_{12}$	5,926,655	4.16
3–6	29.248	1,6-Dimethyl naphthalene	$C_{12}H_{12}$	5,244,910	3.68
3–7	29.769	1,4 + 2,3-Dimethyl naphthalene	$C_{12}H_{12}$	2,348,040	1.65
3–8	29.855	1,5-Dimethyl naphthalene	$C_{12}H_{12}$	1,246,410	0.88
3–9	30.241	1,2-Dimethyl naphthalene	$C_{12}H_{12}$	893,203	0.63
4–1	32.385	1,3,7-Trimethyl naphthalene	$C_{13}H_{14}$	3,088,010	2.17
4–2	32.611	1,3,6-Trimethyl naphthalene	$C_{13}H_{14}$	4,781,094	3.36
4–3	33.048	1,3,5 + 1,4,6-Trimethyl naphthalene	$C_{13}H_{14}$	3,924,889	2.76
4–4	33.209	2,3,6-Trimethyl naphthalene	$C_{13}H_{14}$	3,398,666	2.39
4–5	33.507	1,2,7-Trimethyl naphthalene	$C_{13}H_{14}$	702,950	0.49
4–6	33.578	1,6,7-Trimethyl naphthalene	$C_{13}H_{14}$	2,566,511	1.80
4–7	33.662	1,2,6-Trimethyl naphthalene	$C_{13}H_{14}$	1,638,829	1.15
4–8	34.079	1,2,4-Trimethyl naphthalene	$C_{13}H_{14}$	369,707	0.26
4–9	34.328	1,2,5-Trimethyl naphthalene	$C_{13}H_{14}$	1,502,060	1.05
4–10	34.838	1,2,3-Trimethyl naphthalene	$C_{13}H_{14}$	291,725	0.20
5–1	36.108	1,3,5,7-Tetramethyl naphthalene	$C_{14}H_{16}$	615,333	0.43
5–2	36.648	1,3,6,7-Tetramethyl naphthalene	$C_{14}H_{16}$	1,667,686	1.17
5–3	37.08	1,2,4,6 + 1,2,4,7 + 1,4,6,7-Tetramethyl naphthalene	$C_{14}H_{16}$	1,216,375	0.85
5–4	37.212	1,2,5,7 + 1,3,6,8-Tetramethyl naphthalene	$C_{14}H_{16}$	652,602	0.46
5–5	37.457	2,3,6,7-Tetramethyl naphthalene	$C_{14}H_{16}$	328,699	0.23
5–6	37.685	1,2,6,7-Tetramethyl naphthalene	$C_{14}H_{16}$	642,179	0.45
5–7	37.799	1,2,3,7-Tetramethyl naphthalene	$C_{14}H_{16}$	144,851	0.10
5–8	38.018	1,2,3,6-Tetramethyl naphthalene	$C_{14}H_{16}$	294,758	0.21
5–9	38.466	1,2,5,6 + 1,2,3,5-Tetramethyl naphthalene	$C_{14}H_{16}$	671,250	0.47
6–1	40.005	Phenanthrene	$C_{14}H_{10}$	11,423,674	8.02
7–1	42.929	3-Methyl phenanthrene	$C_{15}H_{12}$	4,602,544	3.23
7–2	43.087	2-Methyl phenanthrene	$C_{15}H_{12}$	5,747,689	4.04
7–3	43.553	9-Methyl phenanthrene	$C_{15}H_{12}$	7,279,250	5.11
7–4	43.701	1-Methyl phenanthrene	$C_{15}H_{12}$	5,730,854	4.02
8–1	45.185	3-Ethyl phenanthrene	$C_{16}H_{14}$	348,234	0.24
8–2	45.518	2-Ethyl phenanthrene	$C_{16}H_{14}$	161,606	0.11
8–3	45.64	9-Ethyl phenanthrene & 3,6-Dimethyl phenanthrene	$C_{16}H_{14}$	1,166,976	0.82
8–4	45.822	3,5-Dimethyl phenanthrene	$C_{16}H_{14}$	1,346,103	0.95
8–5	45.958	2,7-Dimethyl phenanthrene	$C_{16}H_{14}$	976,154	0.69
8–6	46.256	2,10-Dimethyl phenanthrene	$C_{16}H_{14}$	7,201,604	5.06
8–7	46.444	2,5-Dimethyl phenanthrene	$C_{16}H_{14}$	3,616,398	2.54

(continued on next page)

Fig. A1. The total ion chromatogram (TIC) and mass chromatograms showing distributions of aromatic hydrocarbons in the crude oil sample analyzed. (A) The TIC showing relative abundances of aromatic hydrocarbons in the oil sample; (B-F) Mass chromatograms of *m/z* 128, 142, 156, 170 and 180 showing distributions of naphthalene, methylnaphthalene, ethyl- and dimethylnaphthalene, trimethylnaphthalene and tetramethylnaphthalene, respectively; (G–I) Mass chromatograms of *m/z* 178, 192 and 206 showing distributions of phenanthrene, methylphenanthrene and dimethylphenanthrene, respectively; (J–L) Mass chromatograms of *m/z* 184, 198 and 212 showing distributions of dibenzothiophene, methyldibenzothiophene and ethyl- and dimethyldibenzothiophene, respectively; (M-O) Mass chromatograms of *m/z* 168, 182 and 196 showing distributions of dibenzofuran and biphenyl, methyldibenzofuran and dimethyldibenzofuran, respectively; (P–R) Mass chromatograms of *m/z* 166, 180 and 194 showing distributions of fluorene, methylfluorene and dimethylfluorene, respectively; (S) Mass chromatogram of *m/z* 231 showing distributions of triaromatic steroids; (T) Mass chromatogram of *m/z* 245 showing distributions of methyl triaromatic steroids and triaromatic dinosteroids. The labels in the plots represent different compounds. The compound name and content are available in Table A1.

Table A1. (*continued*).

Label No.	Retention time	Compound name	Formular	Peak area	Content in the aromatics (%)
8–8	46.574	1,7-Dimethyl phenanthrene	$C_{16}H_{14}$	4,427,415	3.11
8–9	46.791	2,3 + 1,9-Dimethyl phenanthrene	$C_{16}H_{14}$	2,765,387	1.94
8–10	47.177	1,8-Dimethyl phenanthrene	$C_{16}H_{14}$	853,844	0.60
8–11	47.546	1,2-Dimethyl phenanthrene	$C_{16}H_{14}$	454,849	0.32
9–1	39.234	Dibenzothiophen	$C_{12}H_8S$	392,198	0.28
10–1	41.873	4-Methyl dibenzothiophen	$C_{13}H_{10}S$	1,188,204	0.83
10–2	42.377	3 + 2-Methyl dibenzothiophen	$C_{13}H_{10}S$	392,053	0.28
10–3	42.938	1-Methyl dibenzothiophen	$C_{13}H_{10}S$	128,355	0.09
11–1	44.139	4-Ethyl diphenyl thiophene	$C_{14}H_{12}S$	94,083	0.07
11–2	44.342	4,6-Dimethyl diphenyl thiophene	$C_{14}H_{12}S$	637,810	0.45
11–3	44.702	2,4-Dimethyl diphenyl thiophene	$C_{14}H_{12}S$	322,893	0.23
11–4	44.831	2,6-Dimethyl diphenyl thiophene	$C_{14}H_{12}S$	521,184	0.37
11–5	44.899	3,6-Dimethyl diphenyl thiophene	$C_{14}H_{12}S$	505,693	0.36
11–6	45.334	2,7 + 3,7-Dimethyl diphenyl thiophene	$C_{14}H_{12}S$	140,591	0.10
11–7	45.467	1,6 + 1,4-Dimethyl diphenyl thiophene	$C_{14}H_{12}S$	357,089	0.25
11–8	45.767	1,3-Dimethyl diphenyl thiophene	$C_{14}H_{12}S$	57,359	0.04
11–9	45.829	3,4-Dimethyl diphenyl thiophene	$C_{14}H_{12}S$	127,975	0.09
11–10	45.894	1,7-Dimethyl diphenyl thiophene	$C_{14}H_{12}S$	49,347	0.03
11–11	46.247	2,3 + 1,9-Dimethyl diphenyl thiophene	$C_{14}H_{12}S$	37,234	0.03
11–12	47.011	1,2-Dimethyl diphenyl thiophene	$C_{14}H_{12}S$	48,021	0.03
12–1	31.102	3-Methyl biphenyl	$C_{13}H_{12}$	2,695,504	1.89
12–2	31.426	4-Methyl biphenyl	$C_{13}H_{12}$	992,695	0.70
12–3	32.274	Dibenzofuran	$C_{12}H_8O$	309,600	0.22
13–1	35.316	Methyl dibenzofuran	$C_{13}H_{10}O$	324,855	0.23
13–2	35.777	Methyl dibenzofuran	$C_{13}H_{10}O$	276,517	0.19
13–3	36.046	Methyl dibenzofuran	$C_{13}H_{10}O$	415,395	0.29
14–1	38.471	Dimethyl dibenzofuran	$C_{14}H_{12}O$	381,992	0.27
14–2	38.602	Dimethyl dibenzofuran	$C_{14}H_{12}O$	559,394	0.39
14–3	38.899	Dimethyl dibenzofuran	$C_{14}H_{12}O$	431,099	0.30
14–4	39.11	Dimethyl dibenzofuran	$C_{14}H_{12}O$	984,682	0.69
14–5	39.25	Dimethyl dibenzofuran	$C_{14}H_{12}0$	595,752	0.42
15–1	34.309	Fluorene	$C_{13}H_{10}$	2,889,058	2.03
16–1	37.571	Methylfluorene	$C_{14}H_{12}$	1,171,828	0.82
16–2	37.634	2-Methylfluorene	$C_{14}H_{12}$	1,144,393	0.80
16–3	37.783	1-Methylfluorene	$C_{14}H_{12}$	3,186,625	2.24
16–5	38.106	4-Methylfluorene	$C_{14}H_{12}$	701,303	0.49
17–1	40.689	Dimethylfluorene	$C_{15}H_{14}$	1,425,866	1.00
17–2	40.831	Dimethylfluorene	$C_{15}H_{14}$	1,148,412	0.81
17–3	40.977	Dimethylfluorene	$C_{15}H_{14}$	1,983,074	1.39
17–4	41.421	Dimethylfluorene	$C_{15}H_{14}$	1,021,051	0.72
17–5	41.861	Dimethylfluorene	$C_{15}H_{14}$	512,811	0.36
18–1	54.94	C20-Triaromatic steroid	$C_{20}H_{20}$	282,212	0.20
18–2	55.381	C19-Triaromatic steroid	$C_{19}H_{18}$	721,076	0.51
18–3	56.834	C21-Triaromatic steroid	$C_{21}H_{22}$	257,002	0.18
18–4	63.934	C26-Triaromatic steroid (20S)	$C_{26}H_{32}$	64,458	0.05
18–5	65.344	C26-Triaromatic steroid (20R)	$C_{27}H_{34}$	35,977	0.03
18–6	65.437	C27-Triaromatic steroid (20S)	$C_{26}H_{33}$	145,618	0.10
18–7	66.754	C28-Triaromatic steroid (20S)	$C_{28}H_{36}$	204,719	0.14
18–8	67.465	C27-Triaromatic steroid (20R)	$C_{27}H_{34}$	157,209	0.11
18–9	69.39	C28-Triaromatic steroid (20R)	$C2_8H_{36}$	131,734	0.09
19–1	57.876	C21,Methyl Triaromatic steroid	$C_{21}H_{22}$	266,070	0.19
19–2	59.691	C22,Methyl Triaromatic steroid	$C_{22}H_{24}$	205,940	0.14
19–3	66.491	C27,3-Methyl Triaromatic steroid	$C_{27}H_{34}$	23,362	0.02
19–4	67.268	C27,4-Methyl Triaromatic steroid	$C_{27}H_{34}$	36,671	0.03
19–5	68.229	C27 + C28,3-Methyl Triaromatic steroid	C_{27},C_{28}	69,104	0.05
19–6	68.642	C29,Trimethyltriaromatic algal sterane	$C_{29}H_{38}$	21,797	0.02
19–7	69.064	C28,4-Methyl Triaromatic steroid	$C_{28}H_{36}$	156,891	0.11
19–8	69.522	C29,Trimethyltriaromatic algal sterane	$C_{29}H_{38}$	38,760	0.03
19–9	69.732	C29,3-Methyl Triaromatic steroid	$C_{29}H_{38}$	79,454	0.06
19–10	70.358	C29,Trimethyltriaromatic algal sterane	$C_{29}H_{38}$	86,726	0.06
19–11	70.639	C29,4-Methyl Triaromatic steroid	$C_{29}H_{38}$	177,273	0.12

Table A1. (*continued*).

Label No.	Retention time	Compound name	Formular	Peak area	Content in the aromatics (%)
19–12	70.756	C28,3-Methyl Triaromatic steroid	$C_{28}H_{36}$	18,516	0.01
19–13	71.711	C28,3-Methyl Triaromatic steroid	$C_{28}H_{36}$	99,951	0.07
19–14	72.1	C29,Trimethyltriaromatic algal sterane	$C_{29}H_{38}$	76,364	0.05
19–15	72.258	C29,Trimethyltriaromatic algal sterane	$C_{29}H_{38}$	89,046	0.06
19–16	72.978	C29,3-Methyl Triaromatic steroid	$C_{29}H_{38}$	45,043	0.03
19–17	73.342	C29,Trimethyltriaromatic algal sterane	$C_{29}H_{38}$	58,543	0.04
19–18	74.103	C29,4-Methyl Triaromatic steroid	$C_{29}H_{38}$	117,089	0.08
19–19	74.274	C29,Trimethyltriaromatic algal sterane	$C_{29}H_{38}$	120,578	0.08

REFERENCES

Aitken C. M., Jones D. M. and Larter S. R. (2004) Anaerobic hydrocarbon biodegradation in deep subsurface oil reservoirs. *Nature* **431**, 291–294.

Berger G., Lacharpagne J., Velde B., Beaufort D. and Lanson B. (1997) Kinetic constraints on illitization reactions and the effects of organic diagenesis in sandstone/shale sequences. *Appl. Geochem.* **12**, 23–35.

Bjørkum P. A. and Gjelsvik N. (1988) An isochemical model for formation of authigenic kaolinite, K-feldspar and illite in sediments. *J. Sediment. Res.* **58**, 506–511.

Bjørlykke K. and AAgaard P. (1992) *Clay Minerals in North Sea Sandstones: Origin, Diagenesis and Pelrophysics of Clay Minerals in Sandstones*. SEPM Special Publication, pp. 65–79.

Brown G. and Nadeau P. (1984) Crystal structures of clay minerals and related phyllosilicates [and discussion]. *Philos. Trans. R. Soc. B Biol. Sci.* **311**, 221–240.

Bu H., Yuan P., Liu H., Liu D., Liu J., He H., Zhou J., Song H. and Li Z. (2017) Effects of complexation between organic matter (OM) and clay mineral on OM pyrolysis. *Geochimica et Cosmochimica Acta* **212**, 1–15.

Cai J. G., Lu L. F., Bao Y. J., Fan F. and Xu J. L. (2012) The significance and variation characteristics of interlay water in smectite of hydrocarbon source rocks. *Sci. China Earth Sci.* **55**, 397–404.

Carothers W. W. and Kharaka Y. K. (1978) Aliphatic acid anions in oil-field waters–implications for origin of natural gas. *AAPG Bull.* **62**, 2441–2453.

Chen Z. Z. M., Ming Z., Xiaoyu S., Shouchun Z. and Youshu B. (2014) The effects of high pressure on oil-to-gas cracking during laboratory simulation experiments. *J. Pet. Geol* **37**, 143–162.

Cheng B., Chen Z., Chen T., Yang C. and Wang T. G. (2018) Biomarker signatures of the Ediacaran-Early Cambrian origin petroleum from the central Sichuan Basin, South China: implications for source rock characteristics. *Mar. Petrol. Geol.*. https://doi.org/10.1016/j.marpetgeo.2018.05.012.

Cui L., Khramov D. M., Bielawski C. W., Hunter D. L., Yoon P. J. and Paul D. R. (2008) Effect of organoclay purity and degradation on nanocomposite performance, Part 1: Surfactant degradation. *Polymer* **49**, 3751–3761.

Deer W. A., Howie R. A. and Zussman J. (2013) An introduction to the rock-forming minerals. *Mineral. Mag.* **36**, 150–151.

Fu Q., Lu P., Konishi H., Dilmore R., Xu H., Seyfried W. E. and Zhu C. (2009) Coupled alkali-feldspar dissolution and secondary mineral precipitation in batch systems: 1. New experiments at 200 °C and 300 bars. *Chem. Geol.* **258**, 125–135.

Giles M. R. (1986) Constraints on the development of secondary porosity in the subsurface: re-evaluation of processes. *Mar. Pet. Geol.* **3**, 243–255.

Glasmann J. R. (1992) The fate of feldspar in Brent Group reservoirsNorth Sea: a regional synthesis of diagenesis in shallow, intermediate, and deep burial environments. *Geol. Soc. Lond. Spec. Publ.* **61**, 329–350.

Glasmann J. R., Clark R. A., Larter S., Briedis N. and Lundegard P. D. (1989) Diagenesis and Hydrocarbon Accumulation, Brent Sandstone (Jurassic), Bergen High Area, North Sea. *AAPG Bull.* **37**, 1341–1360.

Guo L., Xianming X., Hui T. and Zhiguang S. (2009) Distinguishing gases derived from oil cracking and kerogen maturation: insights from laboratory pyrolysis experiments. *Org Geochem.* **40**, 1074–1084.

Guo X., He S., Liu K., Song G., Wang X. and Shi Z. (2010) Oil generation as the dominant overpressure mechanism in the Cenozoic Dongying depression, Bohai Bay Basin, China. *AAPG Bull.* **94**, 1859–1881.

Haas J. L. (1976) Physical properties of the coexisting phases and thermochemical properties of the H_2O component in boiling NaC1 solutions. *USGS Bull.* **1421-b**.

Head I. M., Jones D. M. and Larter S. R. (2003) Biological activity in the deep subsurface and the origin of heavy oil. *Nature* **426**, 344–352.

Helgeson H. C. (1979) Summary and critique of the thermodynamic properties of rock-forming minerals. *Am. J. Sci. A* **287**, 1–229.

Helgeson H. C., Knox A. M., Owens C. E. and Shock E. L. (1993) Petroleum, oil field waters, and authigenic mineral assemblages are they in metastable equilibrium in hydrocarbon reservoirs. *Geochimica et Cosmochimica Acta* **57**, 3295–3339.

Hesp W. and Rigby D. (1973) The geochemical alteration of hydrocarbons in the presence of water: Erdol Kohel-Erdgas-Petrochem. *Brennstoff-Chemie* **26**, 70–76.

Hill R. J., Tang Y., Kaplan I. R. and Jenden P. D. (1996) The influence of pressure on the thermal cracking of oil. *Energy Fuels* **10**, 873–882.

Hill R. J., Tang Y. and Kaplan I. R. (2003) Insights into oil cracking based on laboratory experiments. *Org. Geochem.* **34**, 1651–1672.

Hu Y., Liu X. and Xu Z. (2003) Role of crystal structure in flotation separation of diaspore from kaolinite, pyrophyllite and illite. *Miner. Eng.* **16**, 219–227.

Jones D. M., Head I. M., Gray N. D., Adams J. J., Rowan A. K., Aitken C. M., Bennett B., Huang H., Brown A. and Bowler B. F. (2008) Crude-oil biodegradation via methanogenesis in subsurface petroleum reservoirs. *Nature* **451**, 176–180.

Lewan M. D. (1997) Experiments on the role of water in petroleum formation. *Geochimica et Cosmochimica Acta* **61**, 3691–3723.

Li Y., Song G., Li W., Guo R., Yang X., Chen Y. and Wenjun A. L. (2010) A fossil oil-reservoir and the gas origin in the lower Sha-4 member of the well Fengshen-1 area, the North Dongying zone of the Jiyang depression. *Oil Gas Geol.* **31**, 173–179.

Li Y., Cai J., Song M., Ji J. and Bao Y. (2016) Influence of organic matter on smectite illitization: a comparison between red and dark mudstones from the Dongying Depression, China. *Am. Mineral.* **101**, 134–145.

Liu W. (2001) Modeling description and spectroscopic evidence of surface acid-base properties of natural illites. *Water Res.* **35**, 4111–4125.

Liu X., Cheng J., Sprik M., Lu X. and Wang R. (2014) Surface acidity of 2: 1-type dioctahedral clay minerals from first principles molecular dynamics simulations. *Geochimica et Cosmochimica Acta* **140**, 410–417.

Liu X., Lu X., Sprik M., Cheng J. and Meijer E. J. (2013) Acidity of edge surface sites of montmorillonite and kaolinite. *Geochimica et Cosmochimica Acta* **117**, 180–190.

Lu P., Fu Q., Seyfried W. E., Hedges S. W., Soong Y., Jones K. and Zhu C. (2013) Coupled alkali feldspar dissolution and secondary mineral precipitation in batch systems – 2: New experiments with supercritical CO_2 and implications for carbon sequestration. *Appl. Geochem.* **30**, 75–90.

Lynch F. L., Mack L. and Land L. S. (1996) Burial diagenesis of illite/smectite in shales and the origins of authigenic quartz and secondary porosity in sandstones. *Geochimica et Cosmochimica Acta* **61**, 1995–2006.

Ma B., Cao Y. and Jia Y. (2017) Feldspar dissolution with implications for reservoir quality in tight gas sandstones: evidence from the Eocene Es4 interval Dongying Depression, Bohai Bay Basin, China. *J. Petrol. Sci. Eng.* **150**, 74–84.

Macquaker J. H. S., Taylor K. G., Keller M. and Polya D. (2014) Compositional controls on early diagenetic pathways in fine-grained sedimentary rocks: implications for predicting unconventional reservoir attributes of mudstones. *AAPG Bull.* **98**, 587–603.

Marchand A., Haszeldine R. S., Smalley P. C., Macaulay C. I. and Fallick A. E. (2001) Evidence for reduced quartz-cementation rates in oil-filled sandstones. *Geology* **29**, 915–918.

Milliken K. L. (1992) Chemical behavior of detrital feldspars in mudrocks versus sandstones, Frio Formation (Oligocene), South Texas. *J. Sediment. Res.* **62**, 790–801.

Molenaar N., Cyziene J., Sliaupa S. and Craven J. (2008) Lack of inhibiting effect of oil emplacement on quartz cementation: evidence from Cambrian reservoir sandstones, Paleozoic Baltic Basin. *Geol. Soc. Am. Bull.* **120**, 1280–1295.

Molenaar N., Felder M., Bär K. and Götz A. E. (2015) What classic greywacke (litharenite) can reveal about feldspar diagenesis: an example from Permian Rotliegend sandstone in Hessen, Germany. *Sed. Geol.* **326**, 79–93.

Palandri J. L. and Kharaka Y. K. (2004) *A Compilation of Rate Parameters of Water-Mineral Interaction Kinetics for Application to Geochemical Modeling*. USGS, Menlo Park, CA.

Pan C., Jiang L., Liu J., Zhang S. and Zhu G. (2010) The effects of calcite and montmorillonite on oil cracking in confined pyrolysis experiments. *Org Geochem.* **41**, 611–626.

Pan C., Jiang L., Liu J., Zhang S. and Zhu G. (2012) The effects of pyrobitumen on oil cracking in confined pyrolysis experiments. *Org Geochem.* **45**, 29–47.

Ping H., Chen H., Song G. and Liu H. (2010) Oil cracking of deep petroleum in Minfeng Sag in North Dongying depression, Bohai Bay Basin, China: evidence from natural fluid inclusions. *J. Earth Sci.* **21**, 455–470.

Price L. C. (1993) Thermal stability of hydrocarbons in nature: limits, evidence, characteristics, and possible controls. *Geochimica et Cosmochimica Acta* **57**, 3261–3280.

Raybaud P., Digne M., Iftimie R., Wellens W., Euzen P. and Toulhoat H. (2001) Morphology and surface properties of boehmite (γ-AlOOH): a density functional theory study. *J. Catal.* **201**, 236–246.

Schulz H. M., van Berk W. and Fu Y. (2015) Water-matters. *GeoExPro* **12**, 86–89.

Seewald J. S. (2001) Aqueous geochemistry of low molecular weight hydrocarbons at elevated temperatures and pressures: constraints from mineral buffered laboratory experiments. *Geochimica et Cosmochimica Acta* **65**, 1641–1664.

Seewald J. S. (2003) Organic-inorganic interactions in petroleum-producing sedimentary basins. *Nature* **426**, 327–333.

Shuai Y., Zhang S., Luo P., Liu J. and Hu G. (2012) Experimental evidence for formation water promoting crude oil cracking to gas. *Chin. Sci. Bull.* **57**, 4587–4593.

Song G. Q., Jiang Y. L. and Liu H. (2009) Pooling history of cracked gas in middle-deep reservoirs in Lijin-Minfeng area of the Dongying Sag. *Nat. Gas. Ind.* **29**, 14–18.

Surdam R. C. and Crossey L. J. (1987) Integrated diagenetic modeling: a process-oriented approach for clastic systems. *Annu. Rev. Earth Planet. Sci.* **15**, 141–170.

Tian H., Xiao X., Wilkins R. W. T., Gan H., Guo L. and Yang L. (2010) Genetic origins of marine gases in the Tazhong area of the Tarim basin NW China: implications from the pyrolysis of marine kerogens and crude oil. *Int. J. Coal Geol.* **82**, 17–26.

Tian H., Wang Z., Xiao Z., Li X. and Xiao X. (2006) Oil cracking to gases: Kinetic modeling and geological significance. *Chin. Sci. Bull.* **51**, 2763–2770.

Tian Y., Cao Y., Wang Y., Jian W., Zhang H. and Geosciences S. O. (2015) Genesis of high-quality reservoirs of fan delta front in lower part of the fourth member of Shahejie Formation in Bonan Subsag. *Earth Sci.* **40**, 2067–2080.

Tsuzuki N., Takeda N., Suzuki M. and Yokoi K. (1999) The kinetic modeling of oil cracking by hydrothermal pyrolysis experiments. *Int. J. Coal Geol.* **39**, 227–250.

Tutolo B. M., Luhmann A. J., Kong X., Saar M. O. and Seyfried W. E. (2015) CO_2 sequestration in feldspar-rich sandstone: coupled evolution of fluid chemistry, mineral reaction rates, and hydrogeochemical properties. *Geochimica et Cosmochimica Acta* **160**, 132–154.

Uguna C. N., Carr A. D., Snape C. E. and Meredith W. (2016) Retardation of oil cracking to gas and pressure induced combination reactions to account for viscous oil in deep petroleum basins: Evidence from oil and *n*-hexadecane pyrolysis at water pressures up to 900bar. *Org Geochem.* **97**, 61–73.

van Berk W., Schulz H. and Fu Y. (2013) Controls on CO2 fate and behavior in the Gullfaks oil field (Norway): how hydrogeochemical modeling can help decipher organic-inorganic interactions. *AAPG Bull.* **97**, 2233–2255.

Wang X. T., Wang T. S., Li Y. X., Chen Y., Yun L. I. and Xiong Y. Q. (2015) Experimental study on the effects of reservoir mediums on crude oil cracking to gas. *Geochimica* **44**, 178–188.

Wang Y. Z., Cao Y. C., Zhang S. M., Li F. L. and Meng F. C. (2016) Genetic mechanisms of secondary pore development zones of Es4x in the north zone of the Minfeng Sag in the Dongying Depression, East China. *Petrol. Sci.* **13**, 1–17.

Waples D. W. (2000) The kinetics of in-reservoir oil destruction and gas formation: constraints from experimental and empirical data, and from thermodynamics. *Org Geochem.* **31**, 553–575.

Worden R. H., Bukar R. and Shell P. (2017) The effect of oil emplacement on quartz cementation in a deeply buried sandstone reservoir. *AAPG Bull.* **1**, 49–75.

Xiao Q., Sun Y. and Zhang Y. (2010) The role of reservoir mediums in natural oil cracking: preliminary experimental results in a confined system. *Chin. Sci. Bull.* **55**, 3787–3793.

Xie L., Sun Y., Uguna C. N., Li Y., Snape C. E. and Meredith W. (2016) Thermal cracking of oil under water pressure up to 900 bar at high thermal maturities. 1. Gas compositions and carbon isotopes. *Energy Fuels* **30**, 2617–2627.

Yang Y., Min Y. and Jun Y. S. (2013) A mechanistic understanding of plagioclase dissolution based on Al occupancy and T-O bond length: from geologic carbon sequestration to ambient conditions. *PCCP* **15**, 18491–18501.

Yuan G., Cao Y., Gluyas J., Cao X. and Zhang W. (2018) Petrography, fluid inclusion, isotope and trace element constraints on the origin of quartz cementation and feldspar

dissolution and the associated fluid evolution in arkosic sandstones. *AAPG Bull.* **102**, 761–792.

Yuan G., Cao Y., Gluyas J., Li X., Xi K., Wang Y., Jia Z., Sun P. and Oxtoby N. H. (2015a) Feldspar dissolution, authigenic clays, and quartz cements in open and closed sandstone geochemical systems during diagenesis: typical examples from two sags in Bohai Bay Basin, East China. *AAPG Bull.* **99**, 2121–2154.

Yuan G., Cao Y., Jia Z., Gluyas J., Yang T., Wang Y. and Xi K. (2015b) Selective dissolution of feldspars in the presence of carbonates: the way to generate secondary pores in buried sandstones by organic CO_2. *Mar. Pet. Geol.* **60**, 105–119.

Yuan G., Cao Y., Gluyas J. and Jia Z. (2017) Reactive transport modeling of coupled feldspar dissolution and secondary mineral precipitation and its implication for diagenetic interaction in sandstones. *Geochimica et Cosmochimica Acta* **207**, 232–255.

Zhang T., Ellis G. S., Walters C. C., Kelemen S. R., Wang K. and Tang Y. (2008) Geochemical signatures of thermochemical sulfate reduction in controlled hydrous pyrolysis experiments. *Org Geochem.* **39**, 308–328.

Zhang T., Ellis G. S., Ma Q., Amrani A. and Tang Y. (2012) Kinetics of uncatalyzed thermochemical sulfate reduction by sulfur-free paraffin. *Geochimica et Cosmochimica Acta* **96**, 1–17.

Zhu C., Lu P., Zheng Z. and Ganor J. (2010) Coupled alkali feldspar dissolution and secondary mineral precipitation in batch systems: 4. Numerical modeling of kinetic reaction paths. *Geochimica et Cosmochimica Acta* **74**, 3963–3983.

Zhu C. and Lu P. (2009) Alkali feldspar dissolution and secondary mineral precipitation in batch systems: 3. Saturation states of product minerals and reaction paths. *Geochimica et Cosmochimica Acta* **73**, 3171–3200.

Associate editor: Thomas Wagner